Recurrent rhinovirus infections in a child with inherited MDA5 deficiency

Ian T. Lamborn,[1,5]* Huie Jing,[1]* Yu Zhang,[1] Scott B. Drutman,[8,9]** Jordan K. Abbott,[6]** Shirin Munir,[2] Sangeeta Bade,[10] Heardley M. Murdock,[1] Celia P. Santos,[2] Linda G. Brock,[2] Evan Masutani,[3] Emmanuel Y. Fordjour,[1] Joshua J. McElwee,[11] Jason D. Hughes,[11] Dave P. Nichols,[7] Aziz Belkadi,[12,13] Andrew J. Oler,[4] Corinne S. Happel,[1] Helen F. Matthews,[3] Laurent Abel,[8,12,13] Peter L. Collins,[2] Kanta Subbarao,[2] Erwin W. Gelfand,[6] Michael J. Ciancanelli,[8] Jean-Laurent Casanova,[8,12,13,14,15] and Helen C. Su[1,5]

[1]Laboratory of Host Defenses, [2]Laboratory of Infectious Diseases, [3]Laboratory of Immunology, and [4]Bioinformatics and Computational Biosciences Branch, National Institute of Allergy and Infectious Diseases, National Institutes of Health, Bethesda, MD
[5]Department of Pathology and Laboratory Medicine, Institute for Immunology, Perelman School of Medicine, University of Pennsylvania, Philadelphia, PA
[6]Immunodeficiency Diagnosis and Treatment Program, Division of Allergy and Immunology and [7]Division of Pediatric Pulmonary Medicine, Department of Pediatrics, National Jewish Health, Denver, CO
[8]St. Giles Laboratory of Human Genetics of Infectious Diseases, Rockefeller Branch, The Rockefeller University, New York, NY
[9]Department of Medicine, Memorial Sloan-Kettering Cancer Center, New York, NY
[10]Medical Science & Computing, LLC, Rockville, MD
[11]Merck Research Laboratories, Merck and Co, Boston, MA
[12]Laboratory of Human Genetics of Infectious Diseases, Necker Branch, Institut National de la Santé et de la Recherche Médicale UMR1163 and [13]Paris Descartes University, Imagine Institute, Necker Hospital for Sick Children, Paris, France
[14]Pediatric Immuno-Hematology Unit, Necker Hospital for Sick Children, AP-HP, Paris, France
[15]Howard Hughes Medical Institute, New York, NY

MDA5 is a cytosolic sensor of double-stranded RNA (ds)RNA including viral byproducts and intermediates. We studied a child with life-threatening, recurrent respiratory tract infections, caused by viruses including human rhinovirus (HRV), influenza virus, and respiratory syncytial virus (RSV). We identified in her a homozygous missense mutation in *IFIH1* that encodes MDA5. Mutant MDA5 was expressed but did not recognize the synthetic MDA5 agonist/(ds)RNA mimic polyinosinic-polycytidylic acid. When overexpressed, mutant MDA5 failed to drive luciferase activity from the *IFNB1* promoter or promoters containing ISRE or NF-κB sequence motifs. In respiratory epithelial cells or fibroblasts, wild-type but not knockdown of MDA5 restricted HRV infection while increasing IFN-stimulated gene expression and IFN-β/λ. However, wild-type MDA5 did not restrict influenza virus or RSV replication. Moreover, nasal epithelial cells from the patient, or fibroblasts gene-edited to express mutant MDA5, showed increased replication of HRV but not influenza or RSV. Thus, human MDA5 deficiency is a novel inborn error of innate and/or intrinsic immunity that causes impaired (ds)RNA sensing, reduced IFN induction, and susceptibility to the common cold virus.

INTRODUCTION

Acute respiratory infections are the leading cause of acute illness worldwide (Global Burden of Disease Study 2013 Collaborators, 2015). Of these, upper respiratory infections are estimated at 18.8 billion per yr, and lower respiratory infections at 150 million per yr. Most upper respiratory infections, including common colds that are characterized by runny and congested nose, sore throat, and cough, are caused by viruses, with human rhinoviruses (HRV) comprising >100 serotypes identified in up to half of cases (Mäkelä et al., 1998; Heikkinen and Järvinen, 2003; Byington et al., 2015). Although common colds are usually mild and self-limited, they can be complicated by sinus or middle ear infections and croup that also involve other regions of the upper respiratory tract (Greenberg, 2011). They can also spread to cause lower respiratory tract infections such as bronchiolitis and pneumonia, or worsen asthma or chronic obstructive pulmonary disease. Among

*I.T. Lamborn and H. Jing contributed equally to this paper.

**S.B. Drutman and J.K. Abbott contributed equally to this paper.

Correspondence to Helen C. Su: hsu@niaid.nih.gov

Abbreviations used: CARD, caspase activation recruitment domains; CTD, C-terminal domain; DPBS, Dulbecco's PBS; (ds)RNA, double-stranded RNA; HRV, human rhinovirus; ISRE, IFN-stimulated response element; LTA, lipoteichoic acid; MAF, minor allele frequency; MAVS, mitochondrial antiviral-signaling protein; MDA5, melanoma differentiation-associated protein 5; MOI, multiplicity of infection; poly(I:C), polyinosinic-polycytidylic acid; RIG-I, retinoic acid-inducible gene I; RLR, RIG-I-like helicase receptors; RSV, respiratory syncytial virus; SeV, Sendai virus; UTR, untranslated region; WES, whole exome sequencing.

The Rockefeller University Press $30.00
J. Exp. Med. 2017 Vol. 214 No. 7 1949–1972
https://doi.org/10.1084/jem.20161759

lower respiratory infections, influenza virus is identified in ∼4–22% of cases, respiratory syncytial virus (RSV) in ∼30–75%, and HRV in ∼15–50% (Greenberg, 2011; Pavia, 2011; Hasegawa et al., 2014; Jain et al., 2015). Of all commonly circulating respiratory viruses, influenza leads in causing disability and death in hospitalized adults, whereas RSV, followed by HRV, leads in hospitalized infants and children (Gaunt et al., 2011). Influenza, RSV, and HRV are the three leading causes of disease burden in the elderly, further underscoring the pathogenic importance of these viruses (Gaunt et al., 2011).

Host immunity to many viruses, including those targeting the respiratory tract, can be initiated in mice by the RIG-I-like helicase receptors (RLR) melanoma differentiation-associated protein 5 (MDA5) and retinoic acid-inducible gene I (RIG-I). MDA5 and RIG-I, which are encoded by the *IFIH1* and *DDX58* genes, function as intracellular cytosolic sensors of double-stranded (ds)RNA viral replicative intermediates or byproducts. Both sensors send signals through the adaptor mitochondrial antiviral-signaling protein (MAVS, also known as IPS-1, Cardif, and VISA) to activate IFN production and IFN-regulated gene transcription. This can inhibit virus replication and modulate cellular immune responses. MDA5 has a major role in recognizing and limiting picornavirus replication in mice and in vitro in human cells (Gitlin et al., 2006; Kato et al., 2006; Wang et al., 2009, 2010, 2011; Slater et al., 2010; McCartney et al., 2011; Triantafilou et al., 2011; Jin et al., 2012). Together with RIG-I, MDA5 can also recognize and limit replication of other positive sense single-stranded RNA viruses of the coronavirus, calicivirus, and flavivirus families (Loo et al., 2008; McCartney et al., 2008; Roth-Cross et al., 2008; Li et al., 2010; Züst et al., 2011; Errett et al., 2013), (ds)RNA viruses of the orthoreovirus family (Loo et al., 2008), negative sense single-stranded (ss)RNA viruses of the paramyxovirus and orthomyxovirus families (Kato et al., 2006; Shingai et al., 2007; Gitlin et al., 2010; Baños-Lara et al., 2013; Grandvaux et al., 2014; Kim et al., 2014), and even a DNA virus of the poxvirus family (Delaloye et al., 2009; Pichlmair et al., 2009). However, those studies were conducted in vivo in MDA5-deficient mice and in vitro using mouse and human cells. In contrast, the role of MDA5 deficiency in the course of natural infections in humans is not yet known.

RESULTS

Clinical and virologic characterization

We have intensively studied a 5-yr-old child who had recurrent viral respiratory infections requiring frequent hospitalizations (Fig. 1 A; see Clinical description in Materials and methods). At birth, she had a suspected congenital infection, although prenatal infectious screening was normal. At 40 d of age, she had respiratory failure from concurrent HRV/enterovirus and influenza B virus infections, which required mechanical ventilation, including extracorporeal membrane oxygenation. Since then, she has been repeatedly infected with HRV/enteroviruses detected in nasopharyngeal secretions and respiratory distress. She had two more episodes of influenza A (H3 subtype) and adenovirus, infections with three different coronaviruses (OC43, NL63, and HKU1), and one episode each of RSV and parainfluenza virus type 4. Tests for human metapneumovirus were negative. She continues to require supplemental oxygen and had ground glass opacities, but no bronchiectasis on chest-computed tomography. She has had bacterial superinfections of the respiratory tract, but no opportunistic or chronic systemic virus infection, including EBV or CMV. Although she initially had low serum immunoglobulin levels and lymphopenia (effecting T, NK, and B cell subsets), these all normalized between 3 and 4 yr of age. Replacement immunoglobulin therapy, which started at 70 d of age when she was severely ill, was discontinued, and she has since responded with functional antibodies to tetanus, diphtheria, and *Haemophilus influenzae* vaccines. An older brother died of an unknown infectious cause at age one month in a refugee camp. The patient's parents and two other older siblings were healthy.

Because HRV/enterovirus infection preceded the onset of chronic lung disease and HRV/enterovirus infections frequently precipitated hospitalization, we molecularly typed positive samples from the proband. RT-PCR and sequencing of the conserved 5′ UTR used primers that preferentially amplify HRV species A, B, and C and distinguish between HRV and enterovirus (Bochkov et al., 2014). Analysis of PCR-amplified products from seven nasopharyngeal samples collected sequentially from the patient over a 2-yr window demonstrated shedding of HRV-A, but not -B or -C (Fig. 1, B and C). Each sample contained only one HRV-A serotype from 96 clones sequenced, and no two samples (excepting "b" and "c" which were collected within five d of each other) contained the same serotype. Phylogenetic analysis did not reveal any clustering of the identified serotypes (Fig. 1 C). Thus, the frequent detection of HRV/enterovirus was not caused by defective clearance of individual serotypes, but rather resulted from frequent infection with unrelated HRV serotypes.

Genetic analysis

Because the patient was from an isolated small people group of Burma (Myanmar), we hypothesized an autosomal recessive inheritance with a probable founder effect. Whole exome sequencing (WES) was performed on the patient and her healthy immediate relatives, which revealed 1.8% homozygosity in the patient, 2.7% in the mother, and 2.0% in the father. These values were within the upper range of eight previously sequenced exomes from nonconsanguineous individuals (unpublished data) and were consistent with the lack of known consanguinity in this family. When suitable filtering on the variants was performed, a single homozygous missense mutation in *IFIH1* NM_022168.3: c.1093A>G, p.K365E was identified in the patient and confirmed by Sanger dideoxy sequencing (Fig. 2 B; and Tables S1 and S2). This variant (rs117608083) was extremely rare, with an average minor allele frequency (MAF) in the Exome Aggregation Consor-

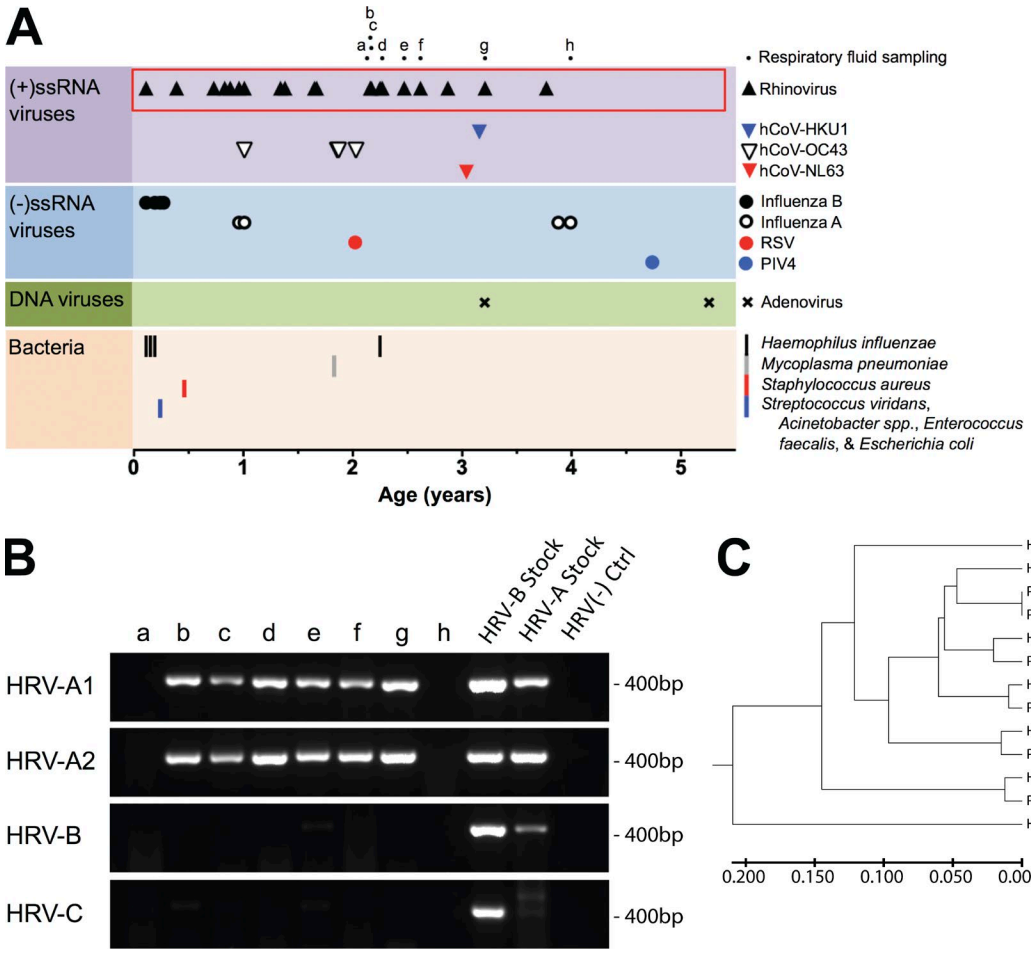

Figure 1. **Infection history in a human with recurrent respiratory tract infections.** (A) Timeline of pathogens recovered from the respiratory tract. These were classified as positive single-stranded RNA virus, negative single-stranded RNA virus, double-stranded DNA virus, or bacteria as indicated in the adjacent symbol key. (B) RT-PCR molecular typing of RNA isolated from nasopharyngeal samples, using primer sets that preferentially amplify the indicated HRV species. Patient's samples a to h, as indicated in A, were collected between 2 and 4 yr of age. Sample a was negative for respiratory pathogens and h positive for influenza A. Purified HRV-B14 and -A16 virus stocks, and a sample from a different subject having respiratory symptoms but negative for HRV/enterovirus, were also tested. Results are representative of three repeats. (C) Phylogenetic tree based on nucleotide sequences of 5′UTR of HRV isolates showing evolutionary relationship of the patient's samples to closest serotypes and representative HRV species.

tium (ExAC) database of 0.06%, where it was found mainly in East and South Asian populations, although no homozygotes were observed. The patient's missense mutation occurred at a location that was conserved across species (PhastCons, 1) and under evolutionary constraint (GERP, 3.96). Substitution of glutamate for lysine resulted in loss of physicochemical conservation (Grantham score, 56) and was predicted to have deleterious effects on protein structure and function (PolyPhen2, 0.998). The patient also carried 14 other homozygous missense mutations, 2 compound heterozygous missense mutations, and 3 de-novo missense mutations, but of these, the *IFIH1* mutation was computationally predicted to be most deleterious (CADD score of 25, surpassing mutation significance cutoff threshold for *IFIH1* of 19.3; Itan et al., 2016), with its normal gene product being highly expressed in immune cells and lung (Table S2). For these reasons, we focused our attention on this variant. Both parents and a brother were carriers of this mutation (Fig. 2 A).

Consequences of the MDA5 mutation

The MDA5 protein encoded by *IFIH1* consists of N-terminal tandem caspase activation recruitment domains (CARD) and a C-terminal domain (CTD), which surround a central tripartite helicase core (Wu et al., 2013). MDA5 forms a "C"-shaped ring encircling (ds)RNA, such that its monomers stack together along the (ds)RNA stem to form long filaments necessary for recognition of viral RNA. Lysine at 365 is located in the Hel1 domain of the helicase core (Fig. 2 B), where it interacts with the 2'-hydroxyl group of ribose in the target RNA backbone (Wu et al., 2013). Substitution with glutamic acid introduces a negative charge that is predicted to abolish the protein–nucleic acid interaction and MDA5

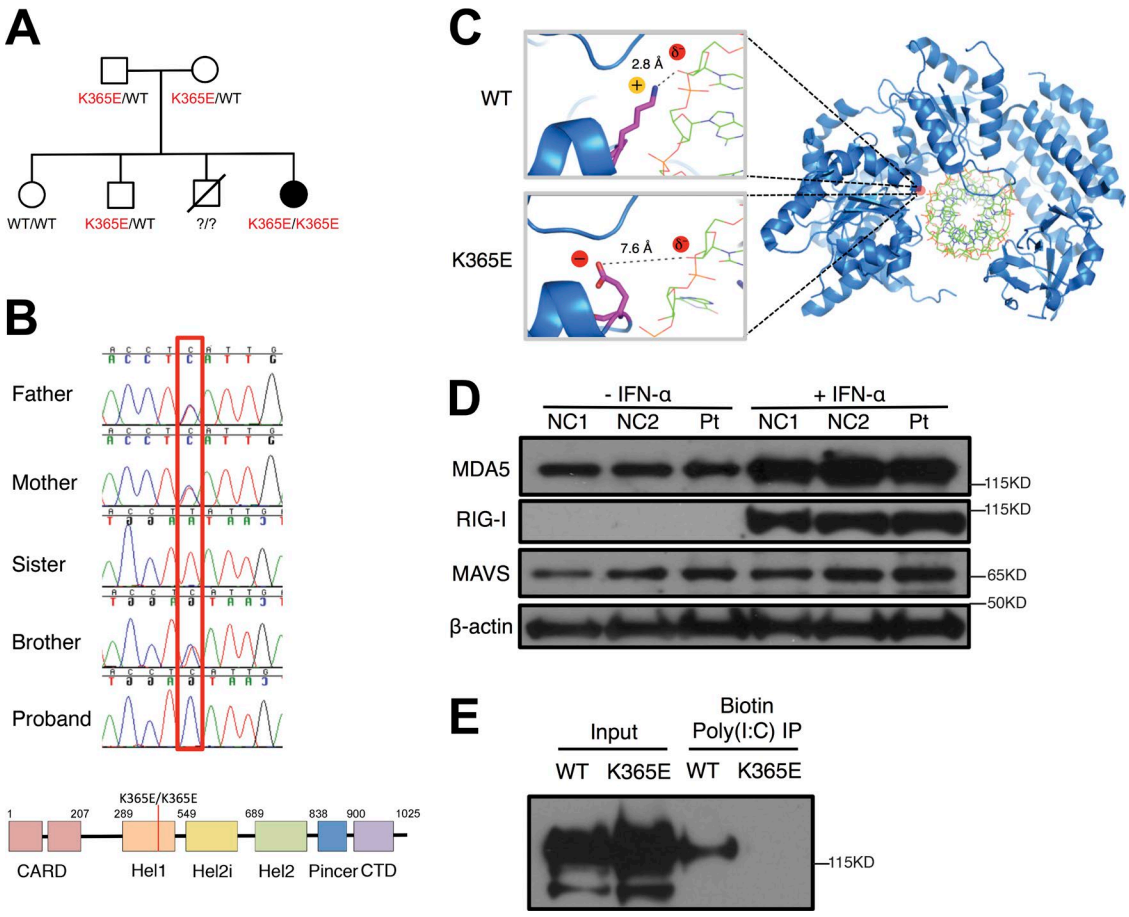

Figure 2. **Autosomal recessive, homozygous *IFIH1* mutation in the proband.** (A) Pedigree indicating genotypes. (B) Confirmatory Sanger sequencing. Schematic below showing mutation location relative to MDA5 protein domains. (C) Ribbon diagram of the MDA5 structure with close-up showing lysine 365 interaction with ribose in RNA, and effects of glutamic acid substitution on distances (Å) between charged groups (yellow sphere, positive; red spheres, negative). (D) Immunoblot of MDA5, RIG-I, and MAVS proteins, relative to β-actin, in cycling T cells, either untreated or treated for 20 h with IFN-α. NC, healthy normal control. Pt, patient. (E) Immunoblot of overexpressed MDA5 (WT or K365E) after affinity precipitation with biotinylated-poly(I:C). D and E are representative of four repeats.

oligomerization (Fig. 2 C). Consistent with our prediction, either before or after induction by IFN-α treatment, the endogenous MDA5 protein in homozygous mutant patient cells was expressed at levels comparable to those in cells from healthy controls or heterozygous or homozygous wild-type family members (Fig. 2 D and not depicted). Levels of endogenous RIG-I or MAVS proteins were unaffected (Fig. 2 D). However, when overexpressed in cells that lack endogenous protein, mutant MDA5 failed to bind to a synthetic MDA5 ligand, poly(I:C) (Fig. 2 E; Gitlin et al., 2006; Kato et al., 2006).

These data suggested that K365E, although normally expressed in patient cells, could not assemble to activate downstream signals. We therefore overexpressed wild-type or mutant MDA5 to test whether they could drive expression of luciferase from several promoters. Cells transfected with wild-type MDA5 increased baseline *IFNB1* promoter activity and further augmented *IFNB1* promoter activity after stimulation with intracellular poly(I:C) (Fig. 3, A and B). In contrast, those cells transfected with the K365E mutant showed minimal activity above nontransfected cells, which did not increase upon stimulation. K365E also failed to drive luciferase activity from IFN-stimulated response element (ISRE)– and NF-κB-driven promoters (Fig. 3, C and D). Notably, the fold induction of luciferase activity of the K365E mutation after poly(I:C) stimulation, relative to that at baseline, was larger than that of wild-type, suggesting that the defect of this mutant lies in MDA5 dimerization or oligomerization upon binding or detecting RNA, although we did not test this further. Co-transfections of the mutant with wild-type MDA5 showed no dominant-negative effect (Fig. 3, E and F). Although biallelic loss-of-function mutations in *IFIH1* have not been previously identified in humans, monoallelic gain-of-function mutations have been reported in humans with Aicardi-Goutières syndrome (Oda et al., 2014; Rice et al., 2014; Rodero and Crow, 2016), Singleton-Merton syndrome (Rutsch et al., 2015), and systemic lupus erythemato-

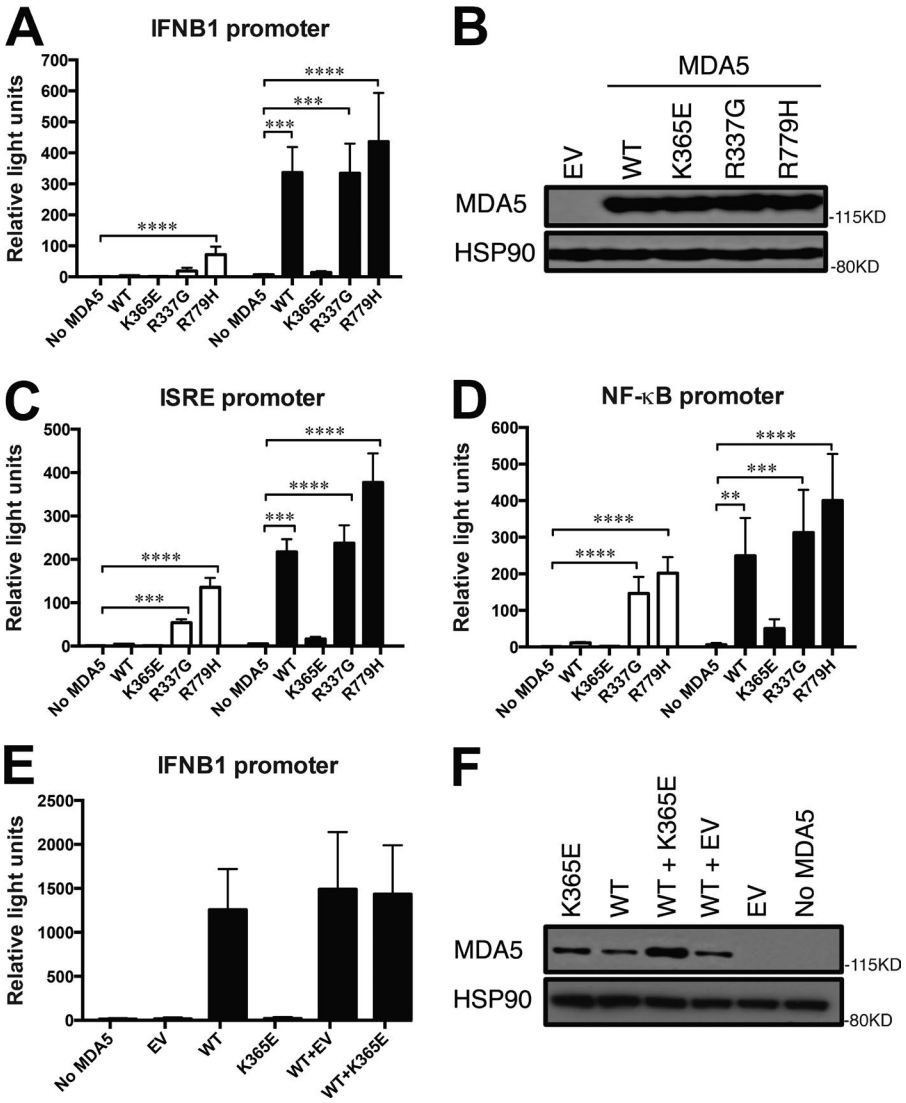

Figure 3. **Loss-of-function *IFIH1* mutation.** (A, C, and D) Relative increase in normalized luciferase activity driven by the *IFNB1* promoter (A), ISRE (C), or NF-κB (D) reporter constructs. Cells were cotransfected with WT or mutant MDA5, and with (filled) or without (open) transfected poly(I:C) as indicated. R337G and R779H are gain-of-function mutants. (B) Immunoblot for MDA5 proteins after transient transfection of 20 ng WT or mutant K365E MDA5, both under CMV promoters. (E) Similar to A, except that cells were cotransfected with 20 ng WT MDA5 (under CMV promoter) and either K365E MDA5 or empty vector (EV; under MSCV promoter). (F) Immunoblot for MDA5 proteins in lysates from E. Data show means ± SD from four (A and E), three (C), and five experiments (D). Data in B and F are examples from experiments shown in A and C–E, respectively. 293T cells lack endogenous MDA5 expression (not depicted). Equivalent lysates from ∼30,000 cells were run across lanes. **, P < 0.01; ***, P < 0.001; ****, P < 0.0001, by one-way ANOVA.

sus with IgA deficiency (Van Eyck et al., 2015). Our patient had neurodevelopmental delay, but lacked the cerebral calcifications or white matter abnormalities characteristic of Aicardi-Goutières syndrome or congenital infection (unpublished data). Moreover, her K365E mutation did not increase luciferase activity, either at baseline or after stimulation, in contrast to the known gain-of-function MDA5 mutants R337G or R779H (Fig. 2, A, C, and D; Rice et al., 2014). Additionally, the patient's cells did not express a type I IFN transcriptional signature characteristic of gain-of-function *IFIH1* mutations (unpublished data; Rice et al., 2013). Thus, we conclude that the K365E missense mutation was loss-of-function.

Virus replication in respiratory epithelial cells

The patient's infection history suggested that MDA5 might function as a general sensor of viruses infecting the respiratory tract in humans, including HRV, RSV, and influenza virus. Alternatively, HRV, as a member of the picornavirus family characterized by a single positive sense strand RNA genome, would be more likely to have extended stretches of RNA double helices during the generation of viral replicative intermediates that might bind effectively to MDA5 (Palmenberg et al., 2009). To test innate immune responses in respiratory epithelium, we infected a transformed respiratory epithelial cell line A549, in which genes of the RLR pathway were silenced by transient transfection of siRNA. Silencing of MDA5, RIG-I, or MAVS expression increased both HRV transcripts and production of infectious virus (Fig. 4, A–F; and Fig. S1, A and B). The requirement for MDA5 or MAVS in optimal virus control occurred not only for HRV-B (Fig. 4, A–F; and Fig. S1, A and B), but also for HRV-A in human primary fibroblasts (Fig. 4, G and H; and Fig. S1 C). In A549 cells, HRV minimally induced low levels of IFN-regulated transcripts, which were decreased upon MDA5 silencing, consistent with further impairment in virus recognition and antiviral responses (Fig. 5, A and B). Both IFN-β (*IFNB1*)

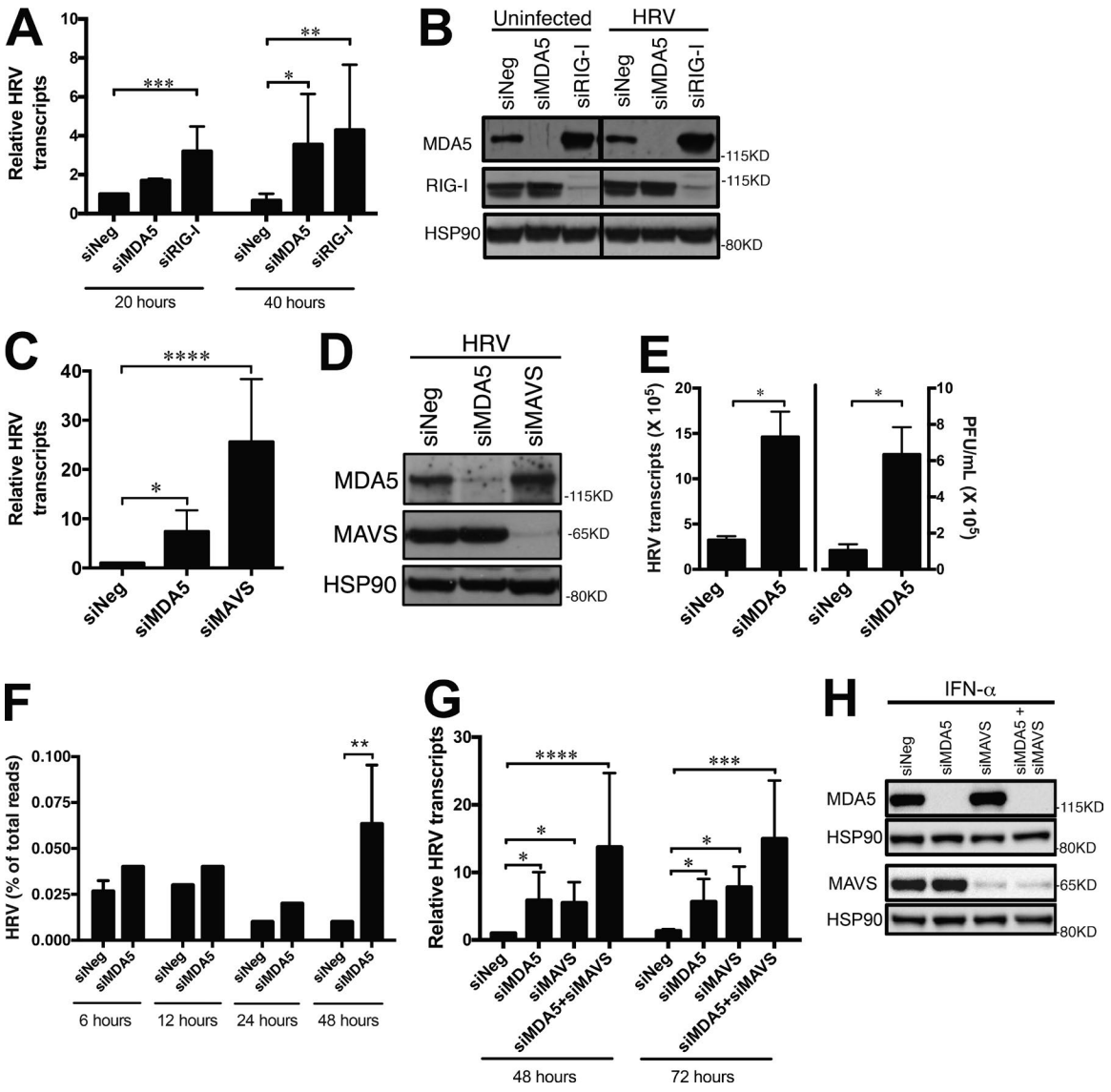

Figure 4. **Loss of MDA5 function results in increased replication of HRV in respiratory epithelial cells.** (A) HRV transcripts, normalized to nonspecific siRNA negative (siNeg) control at 20 h. HRV-B14–infected (MOI: 1) A549 cells were previously transfected with the indicated siRNA. (B) Immunoblot showing efficiencies of MDA5 and RIG-I knockdown in A. Transfected cells were left uninfected or infected with HRV-B14 for 48 h. 120 µg of lysates were run per lane. (C) Similar to A, at 48 h after infection and two rounds of transient transfection with the indicated siRNA. (D) Immunoblot showing efficiencies of MAVS and MDA5 knockdown in C. (E) HRV transcripts and HRV simultaneously quantitated by infectious plaque assay, at 60 h after HRV-B14 infection. (F) Number of HRV reads in RNA-seq data during HRV-B14 infection. A549 cells were previously transfected with MDA5 or nonspecific negative control siRNA (siNeg). Mean of triplicate expression ratios from triplicate infections were shown for each time point. (G) HRV transcripts, normalized to nonspecific siRNA negative (siNeg) control at 48 h, HRV-A16–infected (MOI: 10). Human primary fibroblasts were previously transfected with the indicated siRNA. (H) Immunoblot showing efficiencies of MDA5 and MAVS knockdown in G, except that cells were treated overnight with IFN-α. Data show means ± SD from six (A); eight (C), four (E), and seven experiments (G). Representative experiments are shown in B, D, and H. *, $P < 0.05$; **, $P < 0.01$; ***, $P < 0.001$; ****, $P < 0.0001$, by Kruskal-Wallis test (A, C, and G); Mann-Whitney *U* test in (E); and Kolmogorov-Smirnov test (F); other comparisons in A and F were nonsignificant.

and IFN-λ (*IFNL3*, IL-28) transcripts were decreased upon MDA5 or MAVS silencing in primary human fibroblasts infected with HRV (Fig. 5, C–E). Increased HRV replication was also observed in primary respiratory nasal epithelial cells from the patient as compared with healthy controls or her parents (Fig. 6 A and Fig. S1 D). Furthermore, increased HRV replication was observed in SV40-transformed fibroblasts in which CRISPR/Cas9 genome editing had been used to generate single-cell clones either hemizygous for the patient's mutant *IFIH1* allele or completely lacking both *IFIH1* alleles (Fig. 6 B and Fig. S1 E). Importantly, transduction with wild-type but not mutant K365E MDA5 in

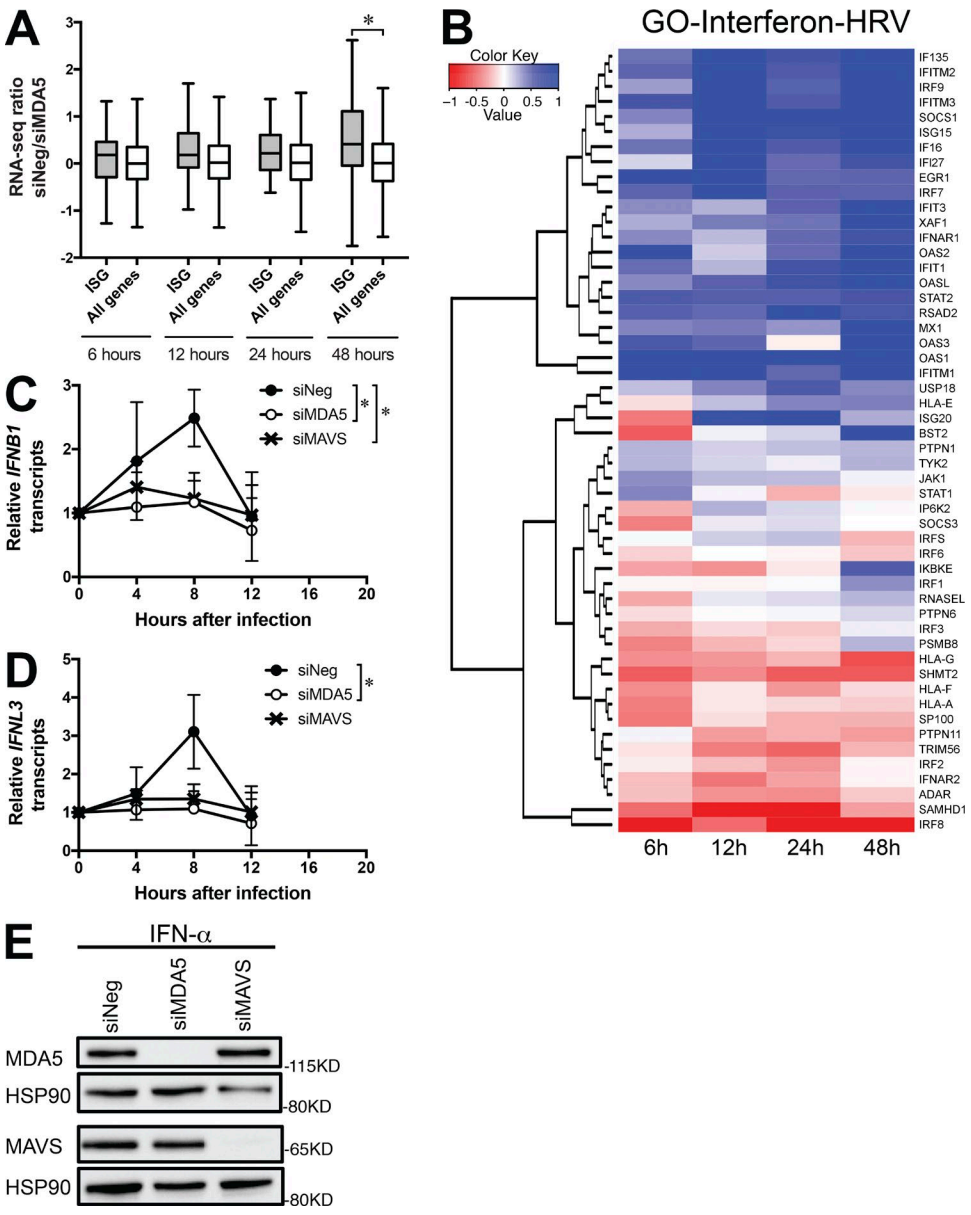

Figure 5. **MDA5 effects on IFN response during HRV infection.** (A) "Response to type I interferon" genes (GO term GO0034340) versus all genes. (B) Heatmap representation of RNA-seq data showing HRV-induced IFN-regulated gene transcripts (RPKM) over the course of infection with HRV-B14 (MOI: 1). Data in A show box-and-whisker plots from triplicate infections. A549 cells were previously transfected with MDA5 or nonspecific negative control siRNA (siNeg) and correspond to Fig. 4 F. Mean of triplicate expression ratios from triplicate infections were shown for each time point in B. *, $P < 0.05$, by Kolmogorov-Smirnov test in A and B; other comparisons were nonsignificant. (C) *IFNB1* transcripts were first normalized to β-actin expression and then shown relative to uninfected cells for each siRNA. HRV-A16-infected (MOI: 10) primary human fibroblasts were previously transfected with the indicated siRNA. (D) Similar to C, except for *IFNL3* (IL-28) transcripts. (E) Immunoblot showing efficiencies of MAVS and MDA5 knockdown in C and D, except that cells were treated overnight with IFN-α. Data show means ± SD from four independent experiments in C and D, and a representative experiment in E. *, $P < 0.05$, by Kruskal-Wallis test comparing areas under the curves in C and D.

A549 cells improved control of HRV replication (Fig. 6, C and D). Thus, these data supported a role for MDA5 in the control of HRV infection in humans and for the patient's recurrent HRV infections.

Although RIG-I is thought to function as the major sensor for the orthomyxoviruses and paramyxoviruses especially in mice, a few studies have suggested a role also for MDA5 in responding to influenza A/B viruses and RSV (Sirén et al., 2006; Loo et al., 2008; Grandvaux et al., 2014; Kim et al., 2014; Benitez et al., 2015). We investigated these possibilities, as the patient had been hospitalized for severe influenza (influenza B in 2011 and influenza A H3N2 in 2011 and 2014)

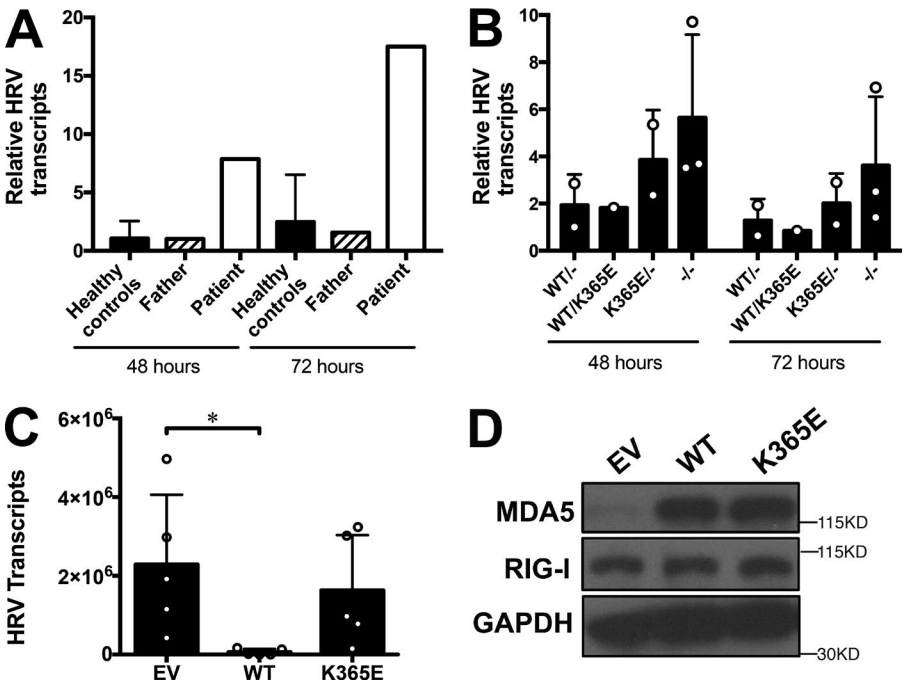

Figure 6. **Loss of MDA5 function results in increased replication of HRV in respiratory epithelial cells and fibroblasts.** (A) HRV transcripts, normalized to father control at 48 h. Primary nasal epithelial cells from the patient, parents, and six normal healthy controls were infected with HRV-B14 (MOI: 1) as indicated. (B) HRV transcripts in maternal fibroblasts, gene-edited to have *IFIH1* genotypes WT/- (2 clones), WT/K365E (1 clone), K365E/- (2 clones), −/− (3 clones), after infection with HRV-B14 (MOI: 1). (C) HRV transcripts in A549 cells previously transduced with empty vector (EV), WT, or K365E MDA5, at 72 h after infection with HRV-B14 (MOI:1). (D) Immunoblot showing MDA5 overexpression and comparable RIG-Iexpression in C. 10.5 µg of lysates were run per lane. Data show means ± SD from two (A), six (B), and five experiments (C). *, $P < 0.05$; ***, $P < 0.001$ by Kruskal-Wallis test; comparisons in B and C were nonsignificant.

and RSV infections. We silenced MDA5, RIG-I, or MAVS expression by transfecting siRNA in A549 cells, which were then infected with a pathogenic influenza A strain (H3N2) isolated in 2011. Consistent with the literature using other influenza virus strains, silencing of either RIG-I or MAVS expression increased influenza transcripts (Fig. 7, A and B; and Fig. S1 F). However, silencing of MDA5 did not increase influenza virus replication, nor did it produce the notable increase in proinflammatory cytokines observed with silencing of RIG-I (Fig. 7, C–F). Infection of primary nasal epithelial cells from the patient also did not show any increased influenza virus replication as compared with her parents (Fig. 8 A and Fig. S1 G). Production of infectious influenza (H1N1) virus was also unaltered in SV40-transformed fibroblasts in which CRISPR/Cas9 genome editing had been used to generate single-cell clones either hemizygous for the patient's mutant *IFIH1* allele or completely lacking both *IFIH1* alleles, in contrast to the increased virus production in cells lacking STAT1 (Fig. 8 B and not depicted). The infected cells that were either hemizygous for the patient's mutant *IFIH1* allele or completely lacking both *IFIH1* alleles did not exhibit increased cytotoxicity or decreased IFN-β production (Fig. 8, C and D). Finally, using a recombinant RSV that expresses enhanced GFP as a marker of virus replication, we observed that silencing MDA5 did not increase RSV transcripts, although it did decrease IFN-regulated transcripts, especially at 6 h, which were more rapidly induced to higher levels than during HRV infection (Fig. 9, A–D). Unlike HRV, RSV transcripts or infectivity and spread were not increased in primary respiratory nasal epithelial cells from the patient (Fig. 9, E and F; and Fig. S1 H). RSV replication was also unaltered in gene-edited fibroblasts either hemizygous for the patient's mutant *IFIH1* allele or completely lacking both *IFIH1* alleles (unpublished data). Together, these results show that under the same conditions where MDA5 deficiency results in increased HRV replication, influenza virus and RSV replication remain unaffected. Hence, MDA5 has a nonredundant role in innate and/or cell-intrinsic immunity against respiratory infections caused by HRV.

IFIH1 variants at the population level

To explore further whether the *IFIH1* variant found in our patient was disease-causing, we analyzed the mutation burden at this locus in the general population. The ExAC database contains 63 loss-of-function (nonsense, splice acceptor/donor, frameshift) and 392 nonsynonymous missense *IFIH1* variants. Of the loss-of-function variants, five had MAF of 0.065% or higher, with homozygotes reported for most of these variants. Homozygotes for the three most frequent loss-of-function variants (rs35732034, rs35337543, and rs35744605) were observed at slightly higher than expected, frequencies in the Icelandic population (Sulem et al., 2015). However, the earliest death of these homozygotes was recorded at 81 yr of age, and there were no childhood deaths from the offspring of heterozygous couples, which are predicted to be 25% homozygotes. No data were available regarding the early medical history of these homozygous individuals, including incidence of childhood HRV or other respiratory virus infections. Given these preexisting data, we determined whether nonsynonymous missense *IFIH1* mutations that compromised function had similar population-level representations. Missense variants having MAF of 0.01% and higher were overexpressed and tested for ability to drive luciferase expression from an *IFNB1* promoter after

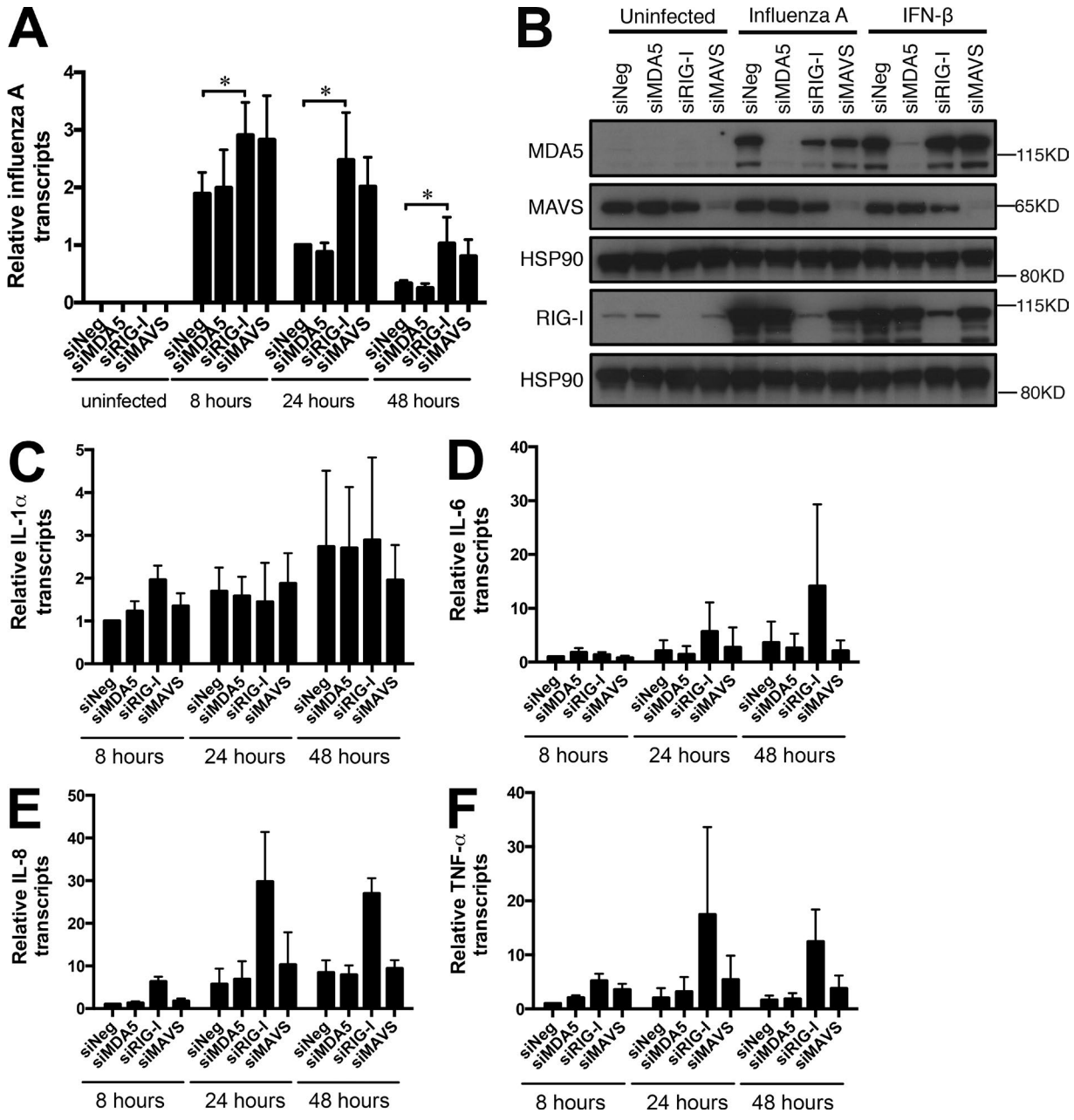

Figure 7. **Loss of MDA5 function does not affect replication of influenza virus or production of proinflammatory cytokines in respiratory epithelial cells.** (A) Influenza (MOI: 0.1) transcripts, normalized to siNeg control at 24 h. Influenza-infected A549 cells were previously transfected with the indicated siRNA. (B) Immunoblotting showing efficiencies of MDA5, RIG-I, and MAVS protein expression, relative to HSP90 loading control, after transient transfection with the indicated siRNA into A549 cells. Transfected cells were left uninfected or infected with influenza strain A/Victoria/361/2011 (MOI: 0.5) for 24 h or treated with IFN-β (10 IU/ml) for 24 h. 20 µg of lysates were run per lane. Shown is a representative experiment corresponding to A. (C–F) Proinflammatory gene transcripts quantitated by qRT-PCR from A. Levels of IL-1α (C), IL-6 (D), IL-8 (E), and TNF (F) were normalized to β-actin and are shown relative to normalized levels at 8 h after infection. Data show means ± SD from six to seven experiments (A) and three independent experiments in (C–F). *, $P < 0.05$, by Kruskal-Wallis test (A); all other comparisons were nonsignificant.

stimulation with intracellular poly(I:C), with loss-of-function (nonsense, splice acceptor/donor, frameshift) and two known gain-of-function variants included for comparison (Fig. 10 and Table S3). Among the 38 missense variants we tested, all showed equivalent protein expression (unpublished data), whereas 11 exhibited >40% decreases in luciferase activity compared with wild-type MDA5, when stimulated by transfected poly(I:C). Although variants demonstrating more

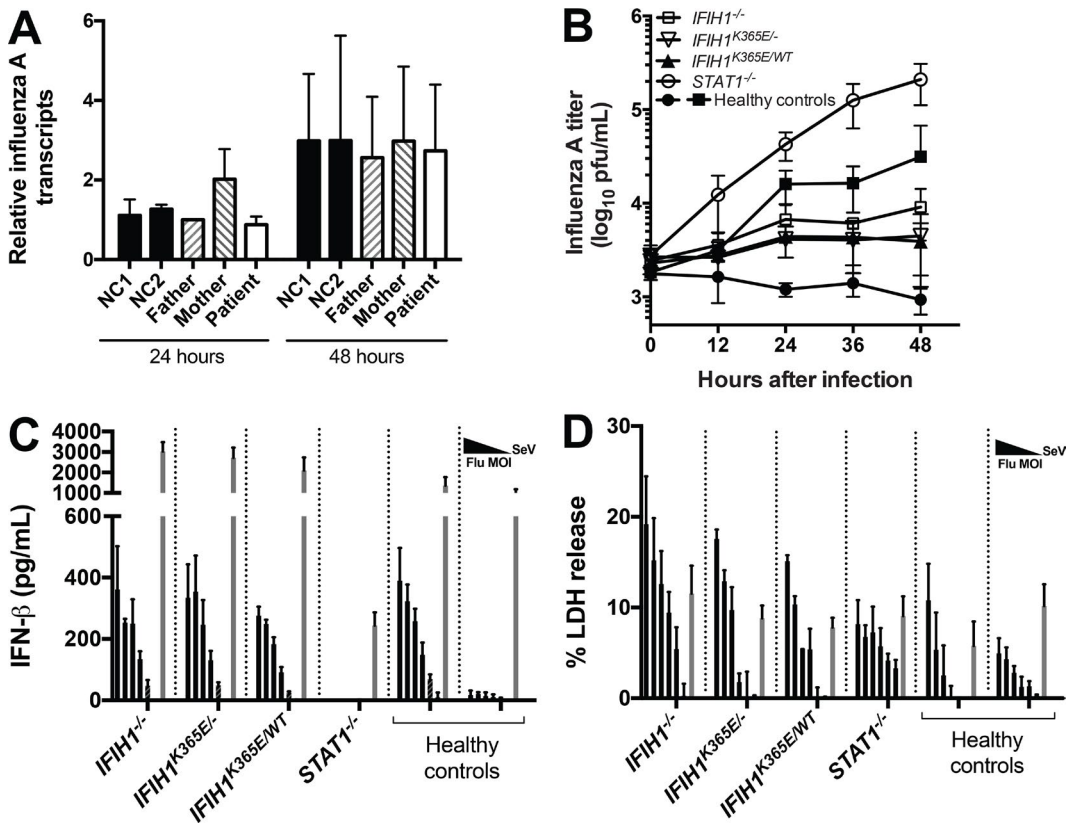

Figure 8. **Loss of MDA5 function does not affect influenza virus replication, or influenza-induced IFN production or cytotoxicity, in respiratory epithelial cells or fibroblasts.** (A) Influenza transcripts, normalized to father control at 24 h. Primary nasal epithelial cells from the patient, parents, and two normal healthy controls were infected with influenza (MOI: 0.02). (B) Influenza virus quantitated by infectious plaque assay, after infection (MOI: 1) of SV40-transformed fibroblasts having the indicated genotypes: empty squares, *IFIH1*$^{-/-}$; empty inverted triangles, *IFIH1*$^{K365E/-}$; solid triangles, *IFIH1*$^{K365E/WT}$; empty circles, *STAT1*$^{-/-}$; solid circles or solid squares, healthy controls. (C) IFN-β released into supernatants as measured by ELISA after infection with influenza strain A/Puerto Rico/8/1934 (MOI: 0.37–54). Decreasing MOI of influenza virus correspond to the bars proceeding from left to right for each cell line. Sendai Virus (SeV) was included as positive control of IFN induction as the right-most bar for each cell line. Genotypes of SV40-transformed fibroblasts are as indicated, with each cell line separated by vertical dotted lines. (D) LDH released into samples from C. Data show means ± SD from four experiments (A) and three independent experiments (B) that are representative of 11 experiments with varying MOIs (0.1–30) and three different influenza strains (A/Netherlands/602/2009, A/California/4/2009, and A/Puerto Rico/8/1934), and three independent experiments (C and D) that are representative of 6 and 7 experiments, respectively, in which the MOI were varied.

severely impaired luciferase activity tended to occur above the mutation significance cutoff, activity levels were generally not well correlated with CADD scores (Fig. 10 A; Itan et al., 2016). The experimentally validated variants having decreased luciferase activity had MAF ranging from 0.01 to 1.1%, and were found in homozygote form in as many as 22 people (Fig. 10 B and Table S3). Furthermore, the presence of complete loss-of-function homozygotes in the population was consistent with little purifying selection. This conclusion was also supported by the computed f-value, which estimates the proportion of nondeleterious nonsynonymous mutations remaining in the population and is inversely proportional to the level of purifying selection (Eilertson et al., 2012). Specifically, the f-values for *IFIH1* and the related RLR sensor *DDX58* were higher than that for *STAT1* (0.5968 and 0.4434, respectively vs. 0.1949), suggesting that the RLR sensors are individually nonessential for the control of most pathogenic viruses (Deschamps et al., 2016). Thus, these data indicate that deleterious *IFIH1* variants exist at rare frequency in the normal population. This implies that there are even rarer homozygous or compound heterozygous individuals, further supporting the role of MDA5 deficiency in our patient's HRV disease, which is a rare infectious phenotype. These data further suggest that other patients with severe HRV disease may carry bi-allelic deleterious variants in *IFIH1*.

DISCUSSION

Studies in single patients can establish causality between genotype and phenotype in humans, provided that the mutant genotype is only found in the affected patient, the specific variant impairs corresponding protein function, and cellular

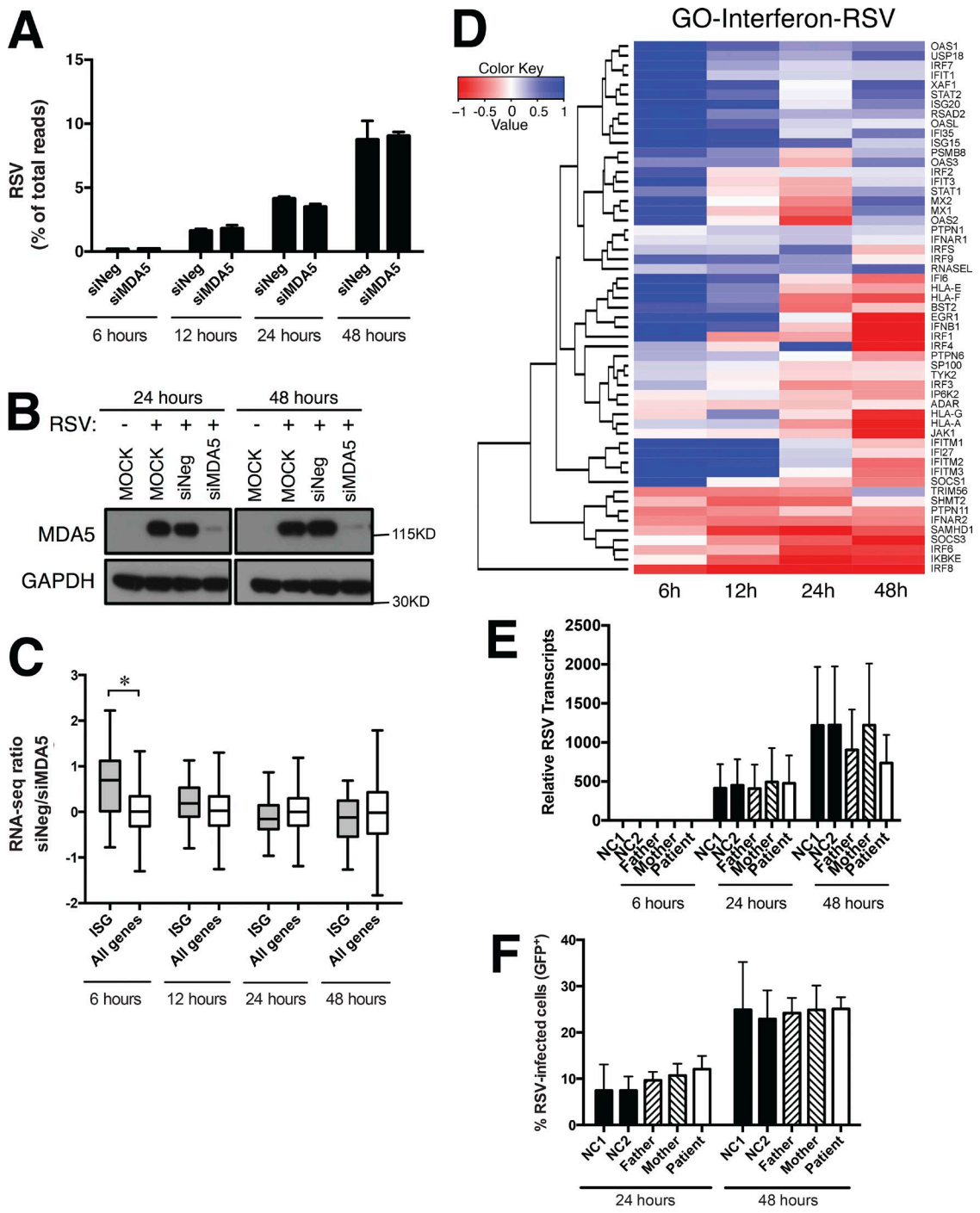

Figure 9. **Loss of MDA5 function does not affect RSV replication, whereas affecting RSV-induced IFN-regulated transcripts.** (A) Number of RSV reads in RNA-seq data during RSV infection. RSV-infected (MOI: 1) A549 cells were previously transfected with MDA5 or nonspecific negative control siRNA (siNeg). (B) Immunoblotting showing efficiencies of MDA5 protein expression, after transient transfection of A549 cells with the indicated siRNA, or without transfection (MOCK). Cells were either left uninfected or infected with RSV, as indicated. 20 µg of lysates were run per lane. Shown is a representative experiment corresponding to A. (C) "Response to type I interferon" genes (GO term GO0034340) versus all genes, from A. (D) Heatmap representation of RNA-seq data showing the expression change between MDA5 siRNA and nonspecific siRNA control of IFN-regulated gene over the course of RSV infection. Mean of triplicate expression ratios from triplicate infections were shown for each time point in A, C, and D. (E) RSV transcripts in primary nasal epithelial cells from the patient (open bar), parents (hatched bars), and two normal healthy controls (solid bars), normalized to father at 6 h, after RSV-GFP infection (MOI: 0.2). (F) Percent GFP^+ of gated live RSV-infected cells from (E). Data show means ± SD from four experiments (E and F). *, $P < 0.05$, by Kruskal-Wallis test (C and D); other comparisons were nonsignificant.

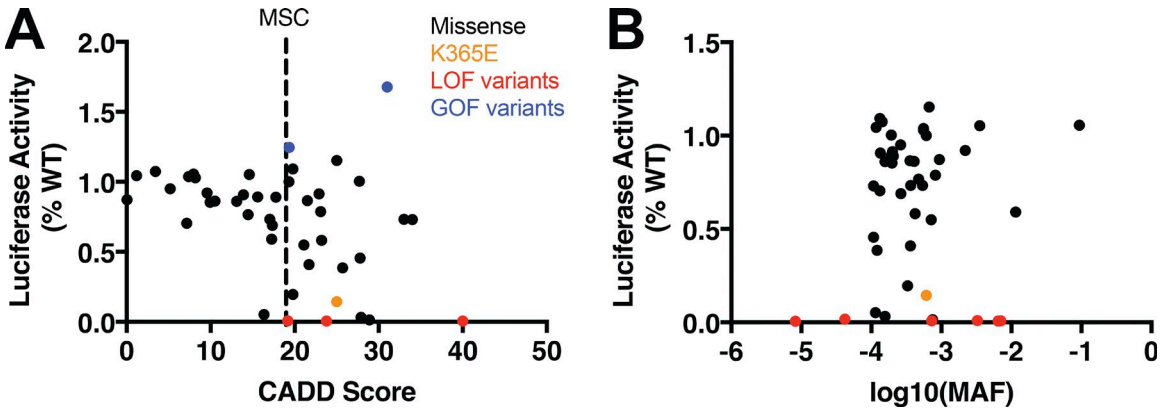

Figure 10. **Functional activity of population-level missense variants in *IFIH1*.** (A) *IFNB1*-driven luciferase activity of overexpressed *IFIH1* variants, measured as means % of the wild-type from at least three independent experiments, plotted against CADD score (A) or MAF (B). Black, missense variants. Orange, patient K365E variant. Red, loss-of-function (nonsense, splice acceptor/donor, frameshift) variants. Blue, gain-of-function variants. MSC, mutation significance cutoff. Variant information with corresponding plotted values (100 ng of construct) are presented in Table S3.

phenotype can be recapitulated or rescued at the molecular level (Casanova et al., 2014; Ciancanelli et al., 2015). By these criteria, we have shown that human MDA5 protects against respiratory infections caused by HRV. HRV accounts for a substantial disease burden of acute lower respiratory infections requiring hospitalization, especially in infants and children where it surpasses that of influenza (Gaunt et al., 2011). Additionally, HRV is primarily responsible for half of upper respiratory infections, but has not been adequately studied as it is often dismissed as innocuous (Heikkinen and Järvinen, 2003; Global Burden of Disease Study 2013 Collaborators, 2015). This has impeded clinical recognition of additional patients with genetic susceptibility to severe respiratory disease associated with the common cold. Whether MDA5 provides physiological protection against other respiratory viruses that we did not test such as human coronaviruses and adenovirus, or against systemic RNA viruses that our patient has not been exposed to such as poliovirus and Hepatitis A virus, is not yet known. Interestingly, our patient has not had hand-foot-mouth disease, nor has she had detectable nonrespiratory enteroviruses associated with acute viral gastroenteritis, possibly due to a differential dependence of MDA5 virus-sensing on the virus or cell type, as well as protective effects of intravenous immunoglobulin treatment that variably contains neutralizing antibodies to enteroviruses (Galama et al., 2000; Arora et al., 2011). The type 1 diabetes mellitus that she developed at two yr of age might have been precipitated by persistent infection with pancreatropic enteroviruses which have been detected in pancreatic autopsy specimens from recent-onset disease (Jaïdane et al., 2010; Rodriguez-Calvo and von Herrath, 2015). Moreover, her intrauterine growth retardation was compatible with congenital infection by untested viruses that might be poorly controlled in multiple organ systems when MDA5 is lacking. Nonetheless, respiratory infections are the most frequent type of infection among the general population, and thus, exposure history most likely accounts for what seems at first glance to be a "site-specific" susceptibility.

Our patient reveals the important protective and nonredundant role MDA5 exerts in the human respiratory tract, where it senses and initiates innate immune responses to HRV. Importantly, by carrying out in vitro infection experiments in MDA5-silenced respiratory epithelial cells—and also in the patient's own MDA5-deficient nasal epithelial cells and gene-edited fibroblasts—we have established that the MDA5 genotype is responsible for the increased HRV replication and HRV clinical phenotype in our patient. In contrast, the lack of in vitro susceptibility to influenza virus or RSV in the same cell types suggests that the MDA5 genotype is not responsible for these infections in our patient. These results also indicate that, surprisingly, other viruses such as influenza virus and RSV, which have (ds)RNA intermediates or byproducts that can be recognized by MDA5, are recognized and controlled by other means when MDA5 is deficient. Although it is possible that defective responses to these other viruses might occur in other MDA5-deficient cell types, our results show that this does not occur at the initial site of infection in the lung within respiratory epithelial cells. Additionally, in our patient, the decreased incidence of infections with age coincided with the maturation of antibody responses. This ability of antibodies to compensate for defective innate immunity is similarly observed in other deficiencies of innate immunity. For example, in IRF7 deficiency associated with isolated influenza susceptibility, the absence of repeated influenza infection was associated with initiation of annual seasonal influenza vaccination (Ciancanelli et al., 2015). Moreover, in TIRAP deficiency associated with isolated staphylococcal susceptibility, staphylococcal lipoteichoic acid (LTA)–specific antibodies were able to prevent disease by rescuing defective TLR2-dependent recognition of LTA (Israel et al., 2017).

HRV is generally considered relatively nonpathogenic when additional factors such as respiratory co-infection or

underlying respiratory disease are absent. Thus, unlike other primary immunodeficiencies characterized by susceptibility to highly pathogenic microbes, the lack of strong purifying selection is not unexpected for MDA5. It is still possible that heterozygous variants that impair activity also exert protective advantage as has been suggested by genome-wide association studies of type 1 diabetes mellitus (Smyth et al., 2006; Nejentsev et al., 2009). As shown by our knockdown experiments, MDA5 function appears to be partially redundant with RIG-I function for controlling HRV replication, where other sensors can contribute to protection when MDA5 function is lacking. Although other genetic variants in the patient might have contributed to her susceptibility to influenza virus or RSV, this seems less likely since replication of influenza virus or RSV in her nasal epithelial cells was comparable to that in cells from healthy controls. Alternatively, it instead seems possible that in the setting of chronic lung disease— which is probably multifactorial from ventilator-induced lung injury, recurrent HRV infections in infancy, or other cofactors—secondary complications including susceptibility to other viruses such as influenza and RSV and bacterial superinfections ensued. Thus, in some individuals, a selective genetic susceptibility to HRV could under certain circumstances contribute more broadly to the pathogenesis of severe respiratory disease during childhood. Furthermore, in light of the known association of HRV infections as a trigger of asthma exacerbations, it will be interesting to explore whether loss-of-function mutations in *IFIH1* are associated with worsened asthma outcome in susceptible individuals.

MATERIALS AND METHODS

Patients

Whole blood, serum, skin biopsies, and nasal airway epithelial scrapings were obtained from the patient, her relatives, or paid healthy volunteers. These individuals gave written informed consent to participate in research protocols approved by Institutional Review Boards at the National Institute of Allergy and Infectious Diseases and National Jewish Health, which are registered in ClinicalTrials.gov under NCT00246857, NCT00128973, and NCT00895271. Buffy coat cells, which were byproducts of volunteer donor blood units, were distributed in an anonymized manner, and thus were exempted from need for informed consent and Institutional Review Board review.

Rhinovirus molecular typing

TRIzol LS reagent (Ambion) was used to extract total RNA from 350 µl of nasopharyngeal washes/aspirates obtained from patients or anonymized controls, or from laboratory virus preparations. 20 µl RNA was reverse-transcribed using a high-capacity cDNA reverse transcription kit with RNase inhibitor (Applied Biosystems). PCR was performed as described previously (Bochkov et al., 2014), except that 32 cycles of a single round of PCR amplification were performed in a 25 µl volume using 2 µl cDNA template and 0.5 µM of forward and reverse primers. The previously published primers, which were relatively species-specific, were used for amplification of the 5′UTR of Rhinovirus (5′UTRn-A1, 5′UTRn-A2, 5′UTRn-B1, and 5′UTRn-Cc, 5′UTR-rev). The PCR-amplified products were resolved by electrophoresis on 2% agarose gel. PCR-amplified products were also purified by QIAquick Gel Extraction kit (QIAGEN) and cloned using TOPO TA Cloning kit for Sequencing (Invitrogen). Plasmid DNA were isolated from transformed TOP10 *E. coli* colonies using the R.E.A.L. Prep 96 Plasmid kit (QIAGEN). For each PCR product, 96 cloned inserts were Sanger dideoxy sequenced using plasmid-specific M13 Forward and Reverse primers. Sequences were analyzed using Sequencher 5.1 software, and BLAST searches of GenBank sequences were performed to identify the virus serotype. The phylogenetic analysis was performed using the UPGMA method of MEGA 7 software, and all positions containing gaps and missing data were eliminated. The phylogenetic trees were drawn to scale, with branch lengths in the same units as those of the evolutionary distances used to infer the phylogenetic tree. The evolutionary distances were computed using the Maximum Composite Likelihood method and are in the units of the number of base substitutions per site. The NCBI HRV reference sequences included in the tree are HRV-A89 (NC_001617.1), HRV-B14 (NC_001490.1), and HRV-C (NC_009996,1).

Genomic analyses

Genomic DNA from the patient and family members were isolated from PBMC using the DNeasy kit (QIAGEN). Whole exome sequencing, using SureSelect Human All Exon 50 Mb kit (Agilent Technologies) coupled with massively parallel sequencing by Illumina HiSeq Sequencing System, was performed using 3 µg of genomic DNA collected from patient, both parents, and an unaffected sister. Sequenced DNA reads were mapped to the hg19 human genome reference by Burrows-Wheeler Aligner with default parameters. Single-nucleotide variant and indel calling were performed using the Genome Analysis Toolkit (Broad Institute). All SNVs/indels were annotated by SeattleSeq Annotation, and an in-house custom analysis pipeline was used to filter and prioritize for nonsynonymous and novel/rare variants (MAF < 0.001) under autosomal recessive or de novo genetic models. UCSC gene sorter Microarray data (GNF Expression Atlas 2 Dta from U133A and GNF1H chips) and Illumina Human BodyMap RNA-seq data were used to prioritize variants for functional validation. For confirmation of *IFIH1* mutations and genotyping of the brother, genomic DNA was PCR-amplified using forward primer 5′-CAATGACACAAATGCCATCA-3′ and reverse primer 5′-CAGGGAGTGGAAAAACCAGA-3′. Sanger dideoxy sequencing of purified PCR-amplified products was performed by the Genomics Unit of the Rocky Mountain Laboratories Research Technologies Section of the

NIAID. The WES data were deposited under dbGaP accession no. phs001235.v1.p1.

Homozygosity was computed as the proportion of the autosomal genome belonging to runs of homozygosity. The runs of homozygosity were defined as ranging at least 1 Mb in length and containing at least 100 SNPs, and were estimated using the homozyg option of the PLINK software (Purcell et al., 2007). The centromeres were excluded because they are long genomic stretches devoid of SNPs and their inclusion might inflate estimates of homozygosity if both flanking SNPs were homozygous. The length of the autosomal genome was fixed at 2,673,768 kb, as previously described (McQuillan et al., 2008).

Molecular modeling

Molecular dynamics simulations were performed using the Assisted Model Building with Energy Refinement (AMBER14) simulation package (Case et al., 2015) with GPU acceleration (Salomon-Ferrer et al., 2013). The FF99SB all-atom potential (Hornak et al., 2006) was used along with parameters for ATP (Meagher et al., 2003) and Zn^{2+} (Li et al., 2013). Starting with the crystal structure of MDA5 (Protein Data Bank ID 4GL2; Wu et al., 2013), ANP was changed to ATP and lysine at position 365 was mutated to glutamic acid in PyMol (The PyMol Molecular Graphics System, Version 1.7.2.1; Schrödinger, LLC). The system was protonated in tleap, solvated with TIP3P explicit water in a periodic truncated octahedron extending 10A beyond the MDA5 complex, neutralized with Na^+, and brought to ∼150 mM of sodium chloride by randomly exchanging solvent molecules with Na^+ or Cl^-. The system was then subjected to energy minimization with diminishing harmonic restraints, followed by heating from 100K to 303K over 30 ps at constant volume with a Berendsen thermostat. Production runs were generated by switching the heated system to a constant pressure and temperature ensemble and allowing the system to equilibrate over 120 ps. All simulations were run in triplicate using the SHAKE algorithm.

Primary T cells

PBMCs were isolated by density centrifugation through Ficoll-Hypaque PLUS (GE Healthcare Life Sciences). Pan T cells were isolated by negative selection using Pan T Cell Isolation kit (Miltenyi Biotec) to ≥98% purity. Pan T cells were stimulated with anti-CD2/CD3/CD28 coated beads from the T Cell Activation/Expansion kit (Miltenyi Biotec), at a bead to cell ratio of 1:1. T cells were cultured in RPMI medium supplemented with 10% FBS (Gibco), 100 U/ml recombinant human IL-2 (Aldesleukin, Prometheus), 2 mM L-glutamine, 100 U/ml penicillin, 100 µg/ml streptomycin (all from Gibco), and 55 µM 2-ME (Sigma-Aldrich). Where indicated, previously activated cycling T cells were treated with 100 IU/ml recombinant human IFN-alpha-2b (Intron A; Merck) for 20 h to induce MDA5 expression.

Primary and SV40-transformed fibroblasts

Fibroblasts were isolated from skin punch biopsies, as previously described (Jing et al., 2014). In brief, dermal and epidermal layers were dissociated after overnight incubation of biopsy tissue with Dispase (BD). The dermis was minced and cultured in complete DMEM-Dulbecco's Modified Eagle Medium (Gibco) supplemented with 10% FBS, 2 mM L-glutamine, 100 U/ml penicillin, 100 µg/ml streptomycin (all from Gibco), and 55 µM 2-ME (Sigma-Aldrich) to allow fibroblasts to grow out. Where indicated, human primary fibroblasts were treated with 100 IU/ml recombinant human IFN-alpha-2b (Intron A; Merck) overnight to induce MDA5 expression. Fibroblasts isolated from a healthy normal donor or the patient's mother were used for *IFIH1* genome editing. Cells from the patient's mother were used to generate wild-type/null, mutant (c.1093A>G, p.K365E)/null, and null/null genotypes. U6gRNA-Cas9-2A-GFP plasmids (HS0000455078; Sigma-Aldrich) were transfected into the fibroblasts using the P3 Primary Cell 96-well Nucleofector kit with Nucleofector Program 96-DT-130 (Lonza). 3 d after transfection, cells highly expressing GFP were single-cell sorted into 96-well plates using a FACSAria Fusion cell sorter (BD) and cultured until confluent. Cells from the patient's mother, or from a healthy normal donor that had not undergone genome editing were also single-cell sorted and cultured in parallel for use as controls. Genotypes for each genome-edited clone were screened by agarose gel electrophoresis of PCR amplified products using forward primer 5′-AAAGGGGAAATACGGAATTGG-3′ and reverse primer 5′-GAGTCAATGACACAAATGCCATC-3′, followed by confirmation by Sanger dideoxy sequencing. Three to five clones each of *IFIH1* genotypes wild-type/null, mutant/null, wild-type/mutant, and null/null were selected and expanded for experiments.

To generate SV40-transformed fibroblast lines, 3×10^6 primary dermal fibroblasts were electroporated in 400 µl of complete DMEM with 3 µg of pLAS plasmid (de Chasseval and de Villartay, 1992) in a 0.4-cm cuvette using the Gene Pulser II electroporation system (1 pulse; 250 V, 1,400 µF, resistance = ∞; Bio-Rad Laboratories). Cells were divided into three 75 cm^2 flasks and monitored 1 to 2 wk for outgrowth of rapidly growing colonies. Cultures were then passaged more than four times to ensure elimination of primary fibroblasts. STAT1-deficient SV40-transformed fibroblasts were described previously (Chapgier et al., 2006).

Primary nasal epithelial cells

Nasal airway epithelial cells were collected from the lower surface of the inferior nasal turbinate using a sterile cytology brush (Cytosoft; Medical Packaging Corporation) as previously described (Poole et al., 2014; Reynolds et al., 2016). Cells were placed in Ham's F-12 medium (Gibco) supplemented with 10% DMSO (Sigma-Aldrich), 30% heat inactivated FBS (Gibco), and 0.1% Y-27632 Rho kinase inhibitor (ApexBio). The collection medium was also supplemented with 1.25 µg/ml amphotericin B (Sigma-Aldrich), 2 µg/ml fluconazole

(Gallipot), and 50 µg/ml gentamicin (Gibco). Cells were stored cryopreserved until needed for culture, using adapted methods that combined use of an irradiated fibroblast feeder layer and Rho kinase inhibition (Suprynowicz et al., 2012). The major modification was the use of irradiated 3T3 fibroblasts (ATCC) as the feeder cell layer. Nasal airway epithelial cells were cultured in T75 flasks to ∼80% confluence and harvested using the previously described multistep trypsinization procedure (Suprynowicz et al., 2012). Harvested cells were cryopreserved using the aforementioned medium but without antibiotic supplementation. Cells of the same passage number and no greater than passage three were used for experiments.

Other cell lines

The human embryonic kidney 293T cell line (ATCC) was cultured in DMEM medium (Gibco) supplemented with 10% FBS (Gibco or Hyclone), 2 mM glutamine, 100 U/ml penicillin, 100 µg/ml streptomycin (all from Gibco), and 55 µM 2-ME (Sigma-Aldrich) for all experiments, or Iscove's Modified Dulbecco's Medium (IMDM; Gibco) supplemented with 10% FBS (Gibco or Hyclone) and 55 µM 2-ME (Sigma-Aldrich) for lentivirus production. The monkey kidney cell line Vero E6 (ATCC) was cultured in DMEM supplemented with 10% FBS, 2 mM glutamine, 100 U/ml penicillin, 100 µg/ml streptomycin, and 55 µM 2-ME. The lung epithelial carcinoma cell line A549 (ATCC) was cultured in F-12K medium (Gibco) supplemented with 10% FBS, 2 mM glutamine, 100 U/ml penicillin, 100 µg/ml streptomycin, and 55 µM 2-ME. The H1-HeLa cell line (gift from W.-M. Lee, Biological Mimetics, Inc., Frederick, MD) was cultured in MEM suspension medium with Earle's salts and no calcium (Gibco), supplemented with 10% FBS (Hyclone), 1x MEM nonessential amino acids, 2 mM L-glutamine, 100 U/ml penicillin, 100 µg/ml streptomycin, 0.1% Pluronic F-68 (all from Gibco), and 55 µM 2-ME (Sigma-Aldrich). H1-Hela cells were maintained in suspension by growth at 37°C on an incubator shaker set at 230 rpm. The Madin-Darby Canine Kidney (MDCK; ATCC) cell line was cultured in DMEM medium (Gibco) supplemented with 10% FBS (Gibco).

Immunoblotting

5 million cells were lysed in 2% SDS or LDS sample loading buffer (Pierce), with 5% 2-ME (Sigma-Aldrich), and heated to 95°C for 10 min. Proteins contained within the supernatants were quantified by BCA (Pierce). Unless otherwise indicated, 40 µg of protein were loaded per lane and were separated on NuPAGE Bis-Tris SDS-PAGE gels with MOPS running buffer (Invitrogen), followed by semi-dry transfer onto nitrocellulose membranes (Bio-Rad Laboratories). After blocking with 5% nonfat dry milk (Bio-Rad Laboratories) in PBS containing 0.1% Tween 20 (Sigma-Aldrich), membranes were incubated with the antibodies directed against MDA5 (clone #D74E4), RIG-I (clone #D14G6), MAVS (clone #3993; all from Cell Signaling Technologies), β-actin (clone #AC-15; Sigma-Aldrich), and HSP90 (clone 68; BD). Signal was detected by incubation with appropriate HRP-conjugated secondary antibodies (Jackson ImmunoResearch Laboratories or Southern Biotech), followed by application of SuperSignal West Pico Chemiluminescent substrate or SuperSignal West Dura Extended Duration Substrate (Thermo Fisher Scientific) and exposing to film.

Plasmids and molecular cloning

Firefly luciferase plasmid driven by the human IFN-β promoter (IFNB-pGL3; Promega; Lin et al., 2000) and the constitutively expressed *Renilla* luciferase reporter plasmid (pRL-TK; Promega) were gifts from Y. He (National Institute of Diabetes and Digestive and Kidney Diseases, Bethesda, MD). The firefly luciferase plasmids driven by the IFN-stimulated response element (pGL4.33-*luc2P*/ISRE/Hygro; Promega) and the NF-κB response element luciferase (pGL4.32-*luc2P*/NF-κB-RE/Hygro; Promega) were modified to express GFP instead of the hygromycin resistance cassette. In brief, pGL4.33-*luc2P*/ISRE/Hygro and pGL4.32-*luc2P*/NF-κB-RE/Hygro plasmids were digested with BamHI and NotI (New England Biolabs) and gel-purified (QIAquick Gel Extraction kit; QIAGEN) to remove the hygromycin resistance cDNA. The coding sequence of EGFP was PCR-amplified from pcDNA3-EGFP (Addgene #13031) using AccuPrime Pfx SuperMix (Invitrogen) and subcloned into the linearized vector backbones using the In-Fusion HD Cloning kit (Clontech), to generate pGL4.33-*luc2P*/ISRE/EGFP and pGL4.32-*luc2P*/NF-κB-RE/EGFP.

pCL20c MSCV-GFP-T2A is a modified version of the lentiviral transfer vector pCL20c MSCV-GFP (Hanawa et al., 2004). In brief, a self-cleavage T2A peptide sequence plus additional restriction sites were added in-frame to the 3′ end of the GFP cDNA from pCL20c MSCV-GFP. This was accomplished by PCR amplification of pCL20c MSCV-GFP using AccuPrime Pfx SuperMix (Invitrogen) with forward primer 5′-CTAGGCGCCGGAATTACCGGTGGC CGGCCGCGGGCCACCATGGTGAGCAAGGGCGAG GAG-3′ and reverse primer 5′-GGCATCGATGCGGCC GCATGCTCACCTGCAGGGGCCGGGGTTCTCCTC CACGTCGCCGCAGGTCAGCAGGCTGCCCCGGCC CTCCTTGTACAGCTCGTCCATGCCGAGAGTGAT CC-3′. The PCR-amplified product was resolved by agarose gel electrophoresis, gel-purified (QIAquick Gel Extraction kit; QIAGEN), and ligated using the In-Fusion HD Cloning kit (Clontech) into the EcoRI- and NotI-digested (New England Biolabs) and gel-purified vector backbone of pCL20c MSCV-GFP (digested and purified to remove the original GFP and multiple cloning site).

The lentiviral transfer vector pLenti-III-UbC/mCherry was generated by replacing the puromycin resistance cDNA in pLenti-III-UbC with mCherry cDNA from pLenti-PGK-mCherry (both from Applied Biological Materials). The mCherry cDNA was PCR-amplified with primers that appended 15 bp that are homologous with the pLenti vector. pLenti-III-UbC/Puro was linearized by restriction digest

with BsiWI. Homologous recombination of the linearized vector and mCherry cDNA was performed by mixing the vector, cDNA, and Cold Fusion Cloning kit master mix (System Biosciences) as per the manufacturer's protocol.

Human *IFIH1* sequence-verified cDNA was purchased from Open Biosystems (clone ID: 40008600) and subcloned into pcDNA3.1 (Invitrogen), pCL20 MSCV GFP T2A (immediately 3′ to T2A sequence), and pLenti-III-UbC/mCherry (under the ubiquitin C promoter) mammalian expression plasmids using the In-Fusion HD Cloning kit (Clontech). Site-directed mutagenesis was used to generate constructs encoding the MDA5 mutants K365E, gain-of-function mutants R337G and R779H, and 38 other MDA5 constructs containing point mutations found in ExAC database with MAF ranging from 0.01 to 9.3%. In brief, wild-type MDA5-expressing plasmids were PCR-amplified using AccuPrime Pfx SuperMix (Invitrogen) and primers containing appropriate point mutations (Table S3). This was followed by Dpn1 digestion (New England Biolabs) and transformation into TOP10 competent cells (Invitrogen). Constructs encoding MDA5, skipping either Exon 8 or Exon 14 because of splicing mutations, were generated using In-Fusion HD Cloning kit. Plasmid DNA was purified using the PureLink HiPure Filter Plasmid kit (Invitrogen), and the introduced mutations were confirmed by Sanger dideoxy sequencing.

Affinity precipitations

500,000 293T cells were seeded per well in tissue culture-treated 6-well plates (Corning). 12–16 h later, cells were transfected with 4 µg of pCL20c MSCV GFP-T2A-WT MDA5, pCL20c MSCV GFP-T2A-K365E MDA5, or pmaxGFP (Lonza), complexed with Lipofectamine 2000 (Invitrogen) according to the manufacturer's recommendations. 48 h later, cells were lysed in 0.05% Nonidet P-40 (Calbiochem), 20 mM Hepes, 1.5 mM magnesium chloride (both from Quality Biological), 150 mM sodium chloride, 0.038% of 2-ME (both from Sigma-Aldrich), and 1x cOmplete EDTA-free protease inhibitor cocktail (Roche). After incubating on ice for 20 min, cell lysates were mechanically disrupted by passing through a 25-gauge needle 10 times. Lysates were centrifuged at 13,200 *g* for 15 min at 4°C, before collecting supernatants. Proteins contained within the supernatants were quantified by BCA (Thermo Fisher Scientific). β,γ-methyleneadenosine 5′-triphosphate (ADPCP; Sigma-Aldrich) was added to 2 mg of protein to a final concentration of 2 mM before adding 1 µg of biotin-labeled high molecular weight (HMW) poly(I:C) (InvivoGen). After incubating at 37°C for 10 min, the mixture was added to M-270 hydrophilic streptavidin Dynabeads (Invitrogen) that had been preblocked for 20 min at 4°C with 600 µg to 1 mg of lysate from pmaxGFP-transfected (Lonza) control 293T cells. After incubation at 4°C for 3 min, the beads were washed three times with lysis buffer containing 2 mM ADP CP. MDA5 protein was eluted by incubating at 95°C for 5 min in 2X SDS buffer protein gel loading solution (Quality Biological) supplemented with 0.3 M sodium chloride and 5% vol/vol 2-ME. Proteins were separated by SDS-PAGE, and immunoblotting for MDA5 was performed as described in the Immunoblotting section.

Luciferase reporter gene assays

50–100,000 293T cells were seeded per well in 24-well tissue culture plates. After culture for 18–24 h to ∼70–80% confluency, Lipofectamine 2000 (Invitrogen) was used for co-transfections of cells with pcDNA3.1 mammalian expression plasmids expressing wild-type MDA5 and/or mutants (20 ng or 100 ng), a firefly luciferase reporter plasmid (200 ng) driven by human IFN-β promoter, and a constitutively expressed *Renilla* luciferase reporter plasmid (20 ng). For some experiments, firefly luciferase reporter plasmids driven by the interferon-stimulated response element (ISRE) or NF-κB response element were instead used. In dominant interference experiments, 20 ng pcDNA3.1 plasmid expressing wild-type MDA5, 100 ng pCL20 MSCV plasmid expressing GFP-T2A-K365E MDA5, and/or 100 ng pCL20 MSCV plasmid expressing GFP-T2A (empty vector) were transfected, along with luciferase reporter plasmids. 6 h later, cells were stimulated with a mixture of 1.2 µg high molecular weight poly(I:C) (InvivoGen) complexed with 1.5 µl Lipofectamine 2000 in 100 µl Opti-MEM I reduced serum medium (Gibco), added to cells for an additional 18–24 h before lysis. The Dual Luciferase Reporter assay (Promega) was used on a Fluostar Omega plate reader (BMG Labtech) to measure luciferase activities contained in cell lysates. Firefly luciferase activity was normalized to *Renilla* luciferase activity. Fold-increase in the normalized activity in MDA5-transfected cells was reported relative to normalized activity in untransfected cells.

HRV stocks

Virus stocks were prepared from HRV-B14 and HRV-A16 seed stocks (a gift from W.-M. Lee) as previously described (Lee et al., 2015a). In brief, H1-HeLa cells were maintained in suspension at 37°C using an incubator shaker set at 230 rpm. Cells were cultured in MEM suspension medium with Earle's salts and no calcium (sMEM; GIBCO BRL #11380-037), supplemented with 10% FBS (Hyclone), 1x MEM nonessential amino acids, 2 mM L-glutamine, 100 U/ml penicillin, 100 µg/ml streptomycin, and 0.1% Pluronic F-68 (Gibco). Cells were incubated with high-titer HRV-B14 at a multiplicity of infection (MOI) of 15, in Dulbecco's PBS (DPBS) containing calcium and magnesium (Lonza) for 1 h at room temperature. After adsorption, infected H1-HeLa cells were cultured in complete medium for an additional 8 h at 35°C, with shaking at 120 rpm. Cell pellets were subjected to three freeze-thaw cycles in 10 mM Hepes, pH 7.2 (Quality Biological), and 0.5% Nonidet P-40 (Calbiochem) added before lysates were clarified by high-speed centrifugation. After incubating clarified lysates with 400 µg RNase A (Invitrogen) for 30 min at 35°C, 0.9% *N*-laurylsarcosine (Sigma-Aldrich) and 28.5 µM 2-ME (Sigma-Aldrich) were added. Virions were concentrated and

partially purified by ultracentrifuging for 2 h at 40,000 rpm, 16°C, over a 30% (wt/vol) sucrose cushion (Sigma-Aldrich) containing 16.7 mM Tris acetate pH 7.5 (Sigma-Aldrich) and 0.833 M sodium chloride (Quality Biological). The virus pellet was resuspended in DPBS containing calcium and magnesium, with 0.01% BSA fraction V (Sigma-Aldrich). Virus aliquots were stored at −80°C until use.

HRV plaque assay

Plaque assays quantitating infectious HRV were performed as previously described, with modifications (Lee et al., 2015b). In brief, HRV-B14 virus stock or cell supernatants were serially diluted in DPBS containing calcium, magnesium, and 0.1% BSA fraction V (Sigma-Aldrich). 200 µl diluted samples were added in duplicate to confluent monolayers of H1-HeLa cells in 6-well plates. After virus adsorption for 1 h at room temperature, the cells were overlaid with 0.8% Noble agar (Sigma-Aldrich) in 1x P6 medium (1x sMEM [Gibco], 26.2 mM sodium bicarbonate, 40.6 mM magnesium chloride hexahydrate, and 0.1% BSA fraction V [Sigma-Aldrich]). Nutritive medium was then overlaid to obtain final concentrations of 1x P6 medium, 2 mM L-glutamine (Gibco), 1.2 mM pyruvic acid (Sigma-Aldrich), 2 mM oxaloacetic acid (Sigma-Aldrich), and 0.1% glucose (Corning). After incubation at 35°C for 2 to 3 d, monolayers were fixed with 10% buffered formalin (Sigma-Aldrich) for 15 min at room temperature, overlaid agar removed, and plaques visualized by staining with 0.1% crystal violet (Sigma-Aldrich) in 20% ethanol for 1 h. Plaques were counted and calculated as PFU/ml of original virus stock or cell supernatant.

HRV Infections

For in vitro infections, A549 cells, seeded at 100,000 per well in 12-well tissue culture plates 1 d prior, were transfected when ∼50–70% confluent with Stealth siRNA to MDA5 (HSS127414), RIG-I (HSS119008), and nonsilencing negative control (Thermo Fisher Scientific) at 40 nM in triplicate wells using siLentFect transfection reagent (Bio-Rad Laboratories). For silencing of MAVS in parallel with controls, cells underwent a second round of Stealth siRNA (HSS183886) transfection 3 d after the first round. After transfection, cells were cultured for 48–72 more h at 37°C before infection. HRV-B14 virus stock, diluted in DPBS containing calcium and magnesium (Lonza), and 0.1% BSA fraction V (Sigma-Aldrich), was added at a MOI of 1. Virus was adsorbed for 1 h at room temperature followed by 1 h at 35°C. After washing five times with DPBS containing calcium and magnesium to remove unbound virus, infected cells were cultured in Ham's F-12K (Kaighn's) medium (Gibco), supplemented with 5% FBS (Hyclone), for 24–72 h at 35°C. Cell supernatants were collected to measure virion release by plaque assay, and total RNA was isolated from cells to measure virus transcripts by qRT-PCR, as described in the Pan-HRV and type I/III IFN qRT-PCR section. In some experiments, A549 cells were transfected with a silencer siRNA to MDA5 (S34498) and Silencer Select Negative Control (Cat# 4390843; Thermo Fisher Scientific) before HRV infection.

In some experiments, human primary dermal fibroblasts were transfected with negative siRNA control, Stealth siRNA to MDA5 (HSS127414), or siRNA to MAVS (Thermo Fisher Scientific; HSS148537), each at 2 µM, using the P3 Primary Cell 96-well Nucleofector kit and Nucleofector Program 96-DT-130 (Lonza). 3 d after transfection, cells were infected with HRV-A16 in DPBS buffer with 0.25% BSA fraction V (Sigma-Aldrich) at MOI of 10. Virus was adsorbed for 1 h at room temperature, and then another h at 35°C. Cells were washed with DPBS and then cultured in DMEM medium supplemented with 10% FBS, 2 mM glutamine, 100 U/ml penicillin, 100 µg/ml streptomycin, and 55 µM 2-ME. Cells were infected for the indicated times. Uninfected cells were used for qRT-PCR normalization purposes, as described below in the next section.

In other experiments, nasal epithelial cells were digested from feeder cells and seeded in 12-well plates at 100,000 cells per well in 1 ml epithelial culture medium (Promocell; C21060) with 10 µM Y-27632 (ApexBio) and incubated at 37°C 5% CO_2. The cells were seeded into plates that had been previously coated with 300 µl rat tail collagen (BD; 354236) at 30 µg/ml in PBS for 45 min at room temperature, washed twice with PBS, and air dried for 20 min. The next d, the cells were washed once with DPBS and then infected with HRV-B14 at a MOI of 1 in DPBS with 0.25% BSA (Sigma-Aldrich). Virus was adsorbed for 40 min at room temperature and then 90 min at 35°C. After washing three times with DPBS, the cells were cultured in epithelial culture medium with 10 µM Y-27632, for 48 or 72 h at 35°C. Total RNA isolated from cells was used to measure virus transcripts by qRT-PCR, as described below in the next section.

Pan-HRV and type I/III IFN qRT-PCR

After washing off nonadherent cells twice with PBS, total RNA was isolated using TRIzol extraction (Invitrogen). 2 µg total RNA was reverse transcribed using High-Capacity cDNA Reverse Transcription kit with RNase Inhibitor (Applied Biosystems). Diluted cDNA was analyzed by quantitative real-time PCR using TaqMan Universal PCR Master Mix on a 7500 Real Time PCR System (Applied Biosystems), as previously described (Lee et al., 2015c). The forward primer D110 was 5′-CTAGCCTGCGTGG-3′, reverse primer RVQ1 was 5′-AAACACGGACACCCAAAGTAGT-3′, and probe RVQ2 was 5′-6FAM-TCCTCCGGCCCC TGA-MGB-NFQ-3′. Viral copy numbers were calculated based upon a standard curve generated from HRV-B14 virion RNA and were shown relative to siRNA negative control. For infection of nasal epithelial cells, viral copy numbers were shown relative to values from father's cells.

For measurement of IFN-β (*IFNB1*) and IFN-λ (*IFNL3*, IL-28), 0.5 µg of total RNA was reverse transcribed using High-Capacity cDNA Reverse Transcription kit with RNase Inhibitor (Applied Biosystems). Diluted cDNA was

analyzed by quantitative real-time PCR using SYBR Green PCR Master Mix on a 7500 Real Time PCR System (Applied Biosystems). The primer sequences used were as follows: *IFNB1* forward primer 5′-CAGGAGAGCAATTTGGAG GA-3′, *IFNB1* reverse primer 5′-CTTTCGAAGCCTTTG CTCTG-3′, *IFNL3* forward primer 5′-TCCTTCAGCAGA AGCGACTC-3′, *IFNL3* reverse primer 5′-GCCACATAG CCCAGTTCAAG-3′, *ACTB* forward primer: 5′-GCACAG AGCCTCGCCTT-3′, *ACTB* reverse primer 5′-GTTGTC GACGACGAGCG-3′. *IFNB1 or IFNL3* transcripts were first normalized to β-actin expression, and then shown as fold-changes relative to 0 h for each siRNA (uninfected cells).

Lentivirus particle production

Specific lentiviral transfer vectors (all in pLenti-III-UbC/mCherry) were constructed as described in the Plasmids and molecular cloning section. VSV-G–pseudotyped lentivirus particles were generated by transient co-transfection into 293T cells of the specific transfer vector together with the packaging plasmids pCMV delta R8.2 (HIV-1 GAG/POL, Tat, and Rev expressing plasmid, Addgene #12263) and pCMV VSV-G (VSV-G envelope expressing plasmid; Addgene #8454; Stewart et al., 2003) using calcium phosphate precipitation (Kingston et al., 2003). In brief, 13 million 293T cells were seeded in poly-L-lysine (Sigma-Aldrich) coated Cell Culture Treated TripleFlasks (Nunc). When cells reached 95% confluency, 250 µg of specific transfer vector, 125 µg pCMV delta R8.2, and 42 µg of pCMV VSV-G were precipitated with calcium phosphate, mixed with 100 ml of complete IMDM, and added to the cells. DNA precipitates were washed out 12 h after transfection and cell supernatants were collected daily for 3 d (stored at 4°C), filtered through 0.22 µm pore-size filter (GE), concentrated by centrifugation at 18,000× g for 3 h at 4°C, and resuspended in Opti-MEM I reduced serum media (Gibco). Lentivirus preparations were stored at −80°C until use.

All lentivirus preparations were titered on 293T cells to determine the concentration of infectious units. 100,000 293T cells were resuspended in complete IMDM containing 8 µg/ml polybrene (Sigma-Aldrich) and 10 µl of diluted lentivirus to a final volume of 1 ml. The suspension was added to a 24-well plate (Corning) and spin-infected at 1,350× g for 30 min at 35°C. 48 h later, cell monolayers were washed twice with PBS, trypsinized (Gibco), transferred to 14 ml round bottom FACS tubes (Falcon), washed with PBS, and resuspended in PBS containing 0.5 µg/ml propidium iodide (Sigma-Aldrich). Single cell suspensions were analyzed on a BD FACSCanto II to determine the percentages of GFP^+ cells among the propidium iodide low (live) populations. Lentivirus dilutions transducing between 2 and 15% of target cells were used to determine concentration of each preparation.

Wild-type *IFIH1* (GenBank accession BC111750), or K365E *IFIH1* cDNA were subcloned under the human ubiquitin C promoter. VSV-G–pseudotyped lentivirus particles were generated by transient co-transfection into 293T cells of the specific transfer vector with the packaging plasmids pCMV delta R8.2 (HIV-1 GAG/POL, Tat, and Rev expressing plasmid) and pVSV-G (VSV-G envelope expressing plasmid; Stewart et al., 2003). Cell supernatants were collected daily for 3 d, filtered through 0.22 µm pore-size filter, concentrated by centrifugation at 18,000× g for 3 h at 4°C, resuspended in Opti-MEM I reduced serum media (Gibco), and stored at −80°C until use.

Assessment of in vitro antiviral function of K365E MDA5

A549 cells, seeded at 50,000 per well in 24-well tissue culture plates 20 h prior, were transduced with lentivirus stocks for 48 h to similar transduction efficiencies (Dittmann et al., 2015). In brief, the cell culture medium was replaced with lentivirus particles diluted in F-12K medium (Gibco) containing 8 µg/ml polybrene (Sigma-Aldrich) and spin-infected at 1,350 *g* for 30 min at 35°C. Transduced cells were infected with HRV-B14 at MOI of 1 for 72 h, as described in the HRV infections section. Transduction efficiencies were assessed by flow cytometry after gating on dead negative–transduced (Zombie Aqua; BioLegend; $mCherry^+$) cells. HRV-B14–infected cultures were washed with DPBS containing calcium and magnesium (Lonza), and pan-HRV qRT-PCR was performed as described in the Pan-HRV and type I/III IFN qRT-PCR section.

Influenza virus stocks

A/Victoria/361/2011 (H3N2), A/California/4/2009 (H1N1), and A/Puerto Rico/8/1934 (H1N1) were propagated in embryonated chicken eggs from virus stocks as previously described (Balish et al., 2013). A/Netherlands/602/2009 was propagated in cell culture on MDCK cells as previously described (Balish et al., 2013). All virus stocks were titered by infectious plaque assay on Madin-Darby Canine Kidney (MDCK) cells (ATCC) as previously described (Balish et al., 2013).

Influenza virus replication

For infection of A549 cells, cells were seeded at 100,000 per well in 12-well tissue culture plates 1 d before and transfected when ∼50–70% confluent with Stealth siRNA targeting MDA5 (HSS127414), RIG-I (HSS119008), MAVS (HSS127415), and nonsilencing negative control (12935300; all from Thermo Fisher Scientific) at 40 nM in triplicate wells using siLentFect transfection reagent (Bio-Rad Laboratories). After transfection, cells were cultured for an additional 72 h at 37°C before infection. Alternatively, primary nasal epithelial cells were digested from feeder cells and seeded in 24-well plates at 100,000 cells per well in 0.5 ml epithelial culture medium (C21060; Promocell) with 10 µM Y-27632 (ApexBio) and incubated at 37°C in 5% CO_2. The cells were seeded on plates previously coated with 150 µl rat tail collagen (354236; BD) at 30 µg/ml in PBS for 45 min at room temperature, washed twice with PBS, and air dried for 20 min. 36 h later, the cells were washed twice with PBS be-

fore infection. Transfected A549 cells were infected with A/Victoria/361/2011 (H3N2) at MOI of 0.1 (diluted in PBS containing 0.3% BSA (Sigma-Aldrich) to a final volume of 300 µl/12-well) for 1 h at room temperature, washed twice with PBS to remove unadsorbed virus, and the medium was replaced with F-12K supplemented with 0.1% BSA, 0.1% FBS (Hyclone), 2 mM glutamine, 55 µM 2-ME, and 1 µg/ml TPCK-trypsin (Sigma-Aldrich). Primary nasal epithelial cells were infected with A/Victoria/361/2011 (H3N2) at MOI: 0.02 (diluted in complete epithelial culture medium without Y-27632 to a final volume of 150 µl/24-well) for 1 h at room temperature, washed twice with PBS to remove unadsorbed virus, and medium was replaced with complete epithelial culture medium plus 1 µg/ml TPCK-trypsin (Sigma-Aldrich) and without Y-27632. After infection, all cultures were returned to 37°C in 5% humidified CO_2.

SV40-transformed fibroblasts were seeded at 50,000 cells/well in 48-well tissue cultures plates in complete DMEM. 16–24 h later, cells were infected with A/Netherlands/602/2009 (H1N1) or A/Puerto Rico/8/1934 (H1N1) at the indicated MOI for 60 min at 37°C in HBSS supplemented with 0.3% BSA (Sigma-Aldrich). Cells were washed twice with PBS and cultured at 37°C in DMEM supplemented with 0.1% FBS (Hyclone) and 0.3% BSA, 2 mM glutamine (Gibco), and 55 µM 2-ME (Sigma-Aldrich) in the presence of 1 µg/ml TPCK-trypsin (Sigma-Aldrich). Cell supernatants were collected at the indicated time points after infection and stored at −80°C. Once all samples were collected, supernatants were thawed and influenza titers were determined by infectious plaque assay on MDCK cells, as previously described (Balish et al., 2013). In brief, MDCK cells were plated in 12-well plates and grown to 100% confluency. Cells were washed twice with PBS, and serial dilutions of influenza infection supernatants diluted in PBS were absorbed onto MDCK cells for 1 h at room temperature. Cells were then overlaid with agar medium of MEM, 28 mM sodium bicarbonate, 2 mM L-glutamine, 100 U/ml penicillin, 100 µg/ml streptomycin (all from Gibco), 0.4% BSA, 1 µg/ml TPCK-trypsin (both from Sigma-Aldrich), and 1% Oxoid Agar (Thermo Fisher Scientific). After 36–60 h, plaques were counted by direct visualization or by fixation and crystal violet counterstain as described in HRV plaque assay, and then calculated as PFU/ml of influenza infection supernatant.

qRT-PCR for influenza-induced proinflammatory cytokines

A549 cells in which MDA5, RIG-I, MAVS, or negative control were silenced by transfecting in siRNA were infected with influenza strain A/Victoria/361/2011 (H3N2) as described above. Total RNA were isolated from influenza-infected A549 cells using TRIzol extraction (Invitrogen). 2 µg total RNA per sample was reverse transcribed using High-Capacity cDNA Reverse Transcription kit with RNase Inhibitor (ABI). All quantitative RT-PCR were performed by the SYBR green method on a 7500 Real Time PCR System (ABI). Primer sequences are as follows: human TNF forward primer, 5′-CTGCTGCACTTTGGAGTGAT-3′; human TNF reverse primer, 5′-AGATGATCTGACTGC CTGGG-3′; human IL-1α forward primer, 5′-ACTGCC CAAGATGAAGACCA-3′; human IL-1α reverse primer, 5′-CCGTGAGTTTCCCAGAAGAA-3′; human IL-6 forward primer, 5′-AGTGAGGAACAAGCCAGAGC-3′; human IL-6 reverse primer, 5′-GTCAGGGGTGGTTATTGCAT-3′; human IL-8 forward primer, 5′-TCCTGATTTCTG CAGCTCTGT-3′; human IL-8 reverse primer, 5′-AAATTT GGGGTGGAAAGGTT-3′; human β-actin forward primer, 5′-GCACAGAGCCTCGCCTT-3′; human β-actin reverse primer, 5′-GTTGTCGACGACGAGCG-3′. The expression of mRNA for proinflammatory cytokine genes of interest was normalized to the expression of β-actin, and then normalized to the control groups at 8 h after infection.

Influenza induced IFN-β and cytotoxicity

SV40-transformed fibroblasts were infected with influenza (A/Puerto Rico/8/1934 [H1N1]) at the indicated MOI for 60 min at 37°C in HBSS supplemented with 0.3% BSA. Cells were washed twice with PBS and cultured at 37°C in DMEM supplemented with 10% FBS. Cell supernatants were collected at the indicated time points after infection. Sendai Virus (SeV) infections were performed in parallel as positive controls, in which cells were infected with 5 hemagglutination units of SeV Cantell strain in DMEM supplemented with 10% FBS and left in the well until the time of collection. For quantitation of IFN-β, supernatants were diluted twofold and were assayed for Human IFN-β using the VeriKine Human Interferon Beta ELISA kit (PBL Assay Science). For quantitation of influenza-induced cytotoxicity, supernatants were diluted 2.5-fold and were assayed for LDH release using the Cytotoxicity Detection kit Plus (Roche) to measure enzymatic activity. Colorimetric absorbance was measured according to kit manufacturers' recommendations, using a VICTOR X4 Multi-label Plate Reader (PerkinElmer).

RSV infections

Recombinant wild-type RSV strain A2 in which enhanced GFP was inserted between the P and M genes was propagated, sucrose-purified, and titered by plaque assay on Vero cells, as previously described (Munir et al., 2008). The virus stock was sequenced and had no adventitious mutations, as confirmed by Sanger dideoxy sequencing. A549 cells were seeded and transfected with siRNA to MDA5, RIG-I, MAVS, or a nonsilencing negative control as described for HRV infections. Alternatively, primary nasal epithelial cells were digested from feeder cells and seeded in 12-well plates at 150,000 cells per well in 1 ml epithelial culture medium (Promocell) with 10 µM Y-27632 (ApexBio) and incubated at 37°C in 5% CO2. The cells were seeded on plates previously coated with 300 µl rat tail collagen (BD) at 30 µg/ml in PBS for 45 min at room temperature, washed twice with PBS, and air dried for 20 min. 36 h later, the cells were washed once with PBS. Transfected A549 cells or primary nasal epithelial

cells were infected with RSV-GFP at an MOI of 1 or 0.2, respectively (diluted in appropriate complete medium, 300 µl per 12-well), for 1 h at room temperature, and washed twice with PBS to remove unadsorbed virus, and then medium was replaced (complete F-12K for A549; epithelial culture media without Y-27632 for nasal epithelial cells) and cultures were returned to 37°C in 5% humidified CO_2.

RSV-GFP qRT-PCR

At 6, 24, or 48 h of RSV-GFP infection, infected cell cultures were washed twice with PBS to remove nonadherent cells, and total RNA was isolated using TRIzol extraction (Invitrogen) according to manufacturer's instructions. 0.5 to 2.0 µg total RNA was reverse transcribed using High-Capacity cDNA Reverse Transcription kit with RNase Inhibitor (Applied Biosystems). Diluted cDNA (1:5 to 1:10 in H_2O) was analyzed for RSV N gene transcripts by quantitative real-time PCR using TaqMan Universal PCR Master Mix on a 7500 Real Time PCR System (Applied Biosystems) per the manufacturer's instructions. The N gene forward primer sequence was 5′-TGGCATGTTATTAATCACAGAAGATGCT-3′, N gene reverse primer sequence was 5′-TTCTCTTCCTAA CCTAGACATCGCATA-3′, and the N gene probe sequence was 5′-6FAM-AACCCAGTGAATTTATG-MGB-NFQ-3′. Viral copy numbers were calculated based upon a standard curve generated from RSV-GFP virion RNA and were shown relative to the RSV transcript levels in the father's cells.

RSV-GFP flow cytometry

At 24 and 48 h after RSV-GFP infection, whole well contents were collected for flow cytometric analysis. First, cell supernatants followed by sequential PBS washes were collected in 5 ml FACS tubes (Falcon). Next, single-cell suspensions were collected after treating with 0.25% trypsin/EDTA (Gibco) for 10 min and combining with cell supernatants and washes. Contents were washed 1 time with PBS and stained with LIVE/DEAD Fixable Near-IR Dead Cell Stain (Molecular Probes) or Zombie NIR Fixable Viability kit (BioLegend) for 20 min at room temperature, fixed in BD Cytofix/Cytoperm solution (BD) or 1% paraformaldehyde (Electron Microscopy Sciences) in PBS for 20 min, washed, and resuspended in PBS containing 1% FCS or 1% BSA and 0.09% sodium azide. The stained and fixed cells were acquired on a BD FACS Canto II or BD LSR II flow cytometers without compensation controls given the negligible spectral overlap between fluorophores. FlowJo 9.8.3 or 10.0.8 (Tree Star Inc.) software was used to enumerate singlet live cells expressing GFP. The values of % GFP^+ cells treated with siRNA to MDA5 are shown relative to the values for negative control siRNA.

RNA-Seq

A549 cells that had been transfected 48 h earlier with siRNA to MDA5 or nonspecific negative control siRNA, were uninfected or infected for 6, 12, 24, and 48 h with HRV-B14 or RSV, as described in the RSV infections section. For each time point, infections were performed in triplicate. Total cellular RNA were isolated using RNeasy Mini kit (QIAGEN). Multiplexed RNA libraries were prepared using the Truseq RNA sample prep kit (Illumina). In brief, poly(A)-containing mRNA were captured with oligodT beads, fragmented, reverse-transcribed, and the cDNA was ligated to Illumina adapters containing indexing barcodes. Libraries were quantified using KAPA Library Quant kits (KAPA Biosystems), before running on a HiSeq 2000 Sequencing System (Illumina) to produce 50 bp single end reads. Sequencing reads were aligned with ELAND to the human reference genome version hg19. Count data of the annotated transcripts from individual samples were normalized for sequence depth. Analyses of differentially expressed genes were performed using the Statistical R package DESeq2. Sequencing reads were also aligned with Bowtie2 to the HRV-B14 or RSV reference genomes to count the read number corresponding to the virus transcripts. The RNA-seq coverage across the virus transcripts were checked for normal distribution and count data of the virus transcripts were also normalized for overall sequence depth. Fold changes were calculated by comparing the RPKM expression values (Reads Per Kilobase per Million mapped reads) under siNeg vs. siMDA5 conditions. For human genes, $\log_2$-transformed (base 2) expression fold changes from DESeq2 output were analyzed for distribution (box-and-whisker diagrams) and hierarchical clustering (heat map of expression values) using R. "Response to type I interferon" genes were selected based on the GO term definition (GO term GO0034340). The comparisons for the fold change distributions of different gene sets were performed using two sample Kolmogorov-Smirnov tests (KS tests). RNA-seq data were deposited into the NCBI BioProject database and the Sequence Read Archive (SRA) under accession no. PRJNA387035.

Clinical description

In brief, the patient is (at the time of publication) a 5-yr-old girl of Karenni descent, whose infection history is presented below. Other clinical and immune history will be detailed in a separate publication to follow.

At birth (37 wk), she was found to have intrauterine growth retardation. Infection screening during routine prenatal care had indicated past maternal infection with HSV-1, Toxoplasma, and CMV. At 40 d of age, she had an upper respiratory infection that was PCR-positive for both HRV/enterovirus and influenza B virus. She developed respiratory failure, which required mechanical ventilation including extra-corporeal membrane oxygenation. Tracheal aspirates grew out *Haemophilus influenzae*, *Streptococcus viridans*, *Acinetobacter* spp., enterococcus, *Escherichia coli*, and other coliform bacteria. Subsequently, she had more than 15 hospital admissions for respiratory distress precipitated by viral respiratory infections. Multiplex PCR revealed two episodes of influenza A; three prolonged intervals of repeated HRV/

enterovirus recovery; four episodes of coronaviruses (OC43, NL63, HKU1); two episodes of adenovirus; and one each of RSV and human parainfluenza virus type 4. Wedge lung biopsy histology, performed when she was 6 mo of age, revealed adequate alveolar architecture with evidence of chronic small airways disease (mucous stasis and collection of foamy alveolar macrophages), but without evidence of active bronchiolitis, pneumonitis, or other inflammatory processes. She continues to require supplemental oxygen, and had ground glass opacities but no bronchiectasis on chest computed tomography. She has been hospitalized on multiple occasions for coliform urinary tract infection and acute gastroenteritis with dehydration, but without detectable viral pathogens. She had an abscess near her G-tube insertion site that grew out *Klebsiella pneumonia*e and *Enterobacter cloacae.* Although she initially had low serum immunoglobulin levels and decreased lymphocyte counts (affecting T, NK, and B cell subsets), these all normalized between 3 to 4 yr old. Replacement immunoglobulins were discontinued and she has since responded with functional antibodies to tetanus, diphtheria, and *Haemophilus influenzae* vaccines. She has no history of opportunistic or chronic systemic virus infection including EBV or CMV despite serological evidence of past exposure. Additionally, when 2 yr of age, she developed new-onset type 1 diabetes mellitus with detectable GAD65 autoantibodies. She has short stature, low weight, hypotonia, weakness, and delays in motor and language development. Brain MRI has shown low periventricular white matter volume with ventriculomegaly, and structural abnormalities of hippocampus, olfactory bulbs, septum pellucidum, and corpus callosum. High-resolution chromosomal microarray analysis identified a 4-kb deletion on chromosome 2 that included the *TM4SF20* gene. This copy number variant has been associated with language delay, white matter hyperintensities, and varied developmental abnormalities in South Asian populations (Wiszniewski et al., 2013). Several regions of absence of heterozygosity totaling 45 MB on five separate chromosomes were also identified. She also had de novo or rare autosomal recessive variants that were identified in genes highly expressed in the brain (Table S2). The convergence of these multiple genetic problems in our patient illustrate how two or more distinct monogenic diseases can occur in a significant proportion of the population examined by WES (Yang et al., 2013, 2014; Retterer et al., 2016).

Statistical analyses

One-way ANOVA with Dunnett's multiple comparisons, Kruskal-Wallis test with Dunn's multiple comparisons, and Mann-Whitney *U* testing were performed using Prism software (GraphPad). Two sample Kolmogorov-Smirnov testing were performed using the Statistical R package.

Online supplemental material

Fig. S1 shows absolute virus transcripts in representative experiments. Table S1 enumerates WES variants found after each biotinformatics filtering stage. Table S2 lists nonsynonymous rare variants found in the patient. Table S3 lists *IFIH1* population variants and their associated luciferase activities.

ACKNOWLEDGMENTS

We thank the following people: for technical assistance, Hyoungjun Ham and Michael Leney-Greene; for technical advice and reagents, Gary Fahle, Ronald Germain, Yong He, Wei-Ming Lee, and Charles Rice; for clinical assistance and support, Patricia Littel, Martha Marquesen, Arianne Soldatos, and Angela Wang; for helpful discussions and/or critically reading the manuscript, Avinash Bhandoola, Sara Cherry, Michael Lenardo, Pamela Schwartzberg, and Qian Zhang. We also thank the patient, her family, and National Jewish Health staff for participating in this study. The data presented in this work are presented in the main paper and the supplemental material, and are archived under dbGaP database accession no. phs001235.v1 and BioProject accession no. PRJNA387035.

This work was supported by the Intramural Research Program of the National Institute of Allergy and Infectious Diseases, National Institutes of Health, the National Center for Research Resources, and the National Center for Advancing Sciences of the National Institutes of Health (grant 8UL1TR000043), the St. Giles Foundation, the Rockefeller University, and National Jewish Health. S.B. Drutman is supported by T32CA009207, and J.K. Abbot was supported by a fellowship from CSL Behring. I.T. Lamborn is a Medical Scientist Training Program student in the Graduate Program in Immunology at the University of Pennsylvania.

The authors declare no competing financial interests.

Author contributions: Y. Zhang, J.J. McElwee, J.D. Hughes, A. Belkadi, and L. Abel analyzed WES, and Y. Zhang and J.J. McElwee discovered the *IFIH1* mutation. I.T. Lamborn and H.M. Murdock assessed MDA5 expression, E.M. performed molecular modeling, and H.M. Murdock performed immunoprecipitations. S.B., H. Jing, and I.T. Lamborn performed luciferase reporter assays. H. Jing and I.T. Lamborn performed HRV experiments. S. Munir developed methods for A549 siRNA transfections. I.T. Lamborn, S. Munir, and L.B. performed RSV experiments. I.T. Lamborn, S.B. Drutman, M.J. Ciancanelli, C.P. Santos, and H. Jing performed influenza experiments. Y. Zhang and A.J. Oler evaluated transcriptomes. Y. Zhang performed rhinovirus molecular typing for phylogenetic analysis. H.M. Murdock, S. Bade, and E.Y.Fordjour assisted with immunoblotting. I.T. Lamborn, H. Jing, and M.J. Ciancanelli generated CRISPR fibroblast lines, and D.P. Nichols generated nasal epithelial cell lines. J.K. Abbott and E.W. Gelfand cared for the patient, and collected and analyzed clinical data with assistance from H.C. Su and C.S. Happel. H.F. Matthews coordinated clinical study protocol and sample collection. H.C. Su planned and supervised the experimental work and data analyses. J.L. Casanova, M.J. Ciancanelli, K. Subbarao, and P.L. Collins provided advice and assisted in supervising experimental work. H.C. Su and I.T. Lamborn prepared the manuscript. All authors discussed and revised the manuscript.

Submitted: 18 October 2016

Revised: 13 April 2017

Accepted: 26 May 2017

REFERENCES

Arora, R., M. Kaplan, and M. Nelson. 2011. Enterovirus-specific IgG in intravenous immunoglobulin preparations. *Ann. Allergy Asthma Immunol.* 106:544–545. http://dx.doi.org/10.1016/j.anai.2011.03.007

Balish, A.L., J.M. Katz, and A.I. Klimov. 2013. Influenza: propagation, quantification, and storage. *Curr Protoc Microbiol* Chapter 15:Unit 15G 11.

Baños-Lara, M.R., A. Ghosh, and A. Guerrero-Plata. 2013. Critical role of MDA5 in the interferon response induced by human metapneumovirus infection in dendritic cells and in vivo. *J. Virol.* 87:1242–1251. http://dx.doi.org/10.1128/JVI.01213-12

Benitez, A.A., M. Panis, J. Xue, A. Varble, J.V. Shim, A.L. Frick, C.B. López, D. Sachs, and B.R. tenOever. 2015. In Vivo RNAi Screening Identifies MDA5 as a Significant Contributor to the Cellular Defense against Influenza A Virus. *Cell Reports.* 11:1714–1726. http://dx.doi.org/10.1016/j.celrep.2015.05.032

Bochkov, Y.A., K. Grindle, F. Vang, M.D. Evans, and J.E. Gern. 2014. Improved molecular typing assay for rhinovirus species A, B, and C. *J. Clin. Microbiol.* 52:2461–2471. http://dx.doi.org/10.1128/JCM.00075-14

Byington, C.L., K. Ampofo, C. Stockmann, F.R. Adler, A. Herbener, T. Miller, X. Sheng, A.J. Blaschke, R. Crisp, and A.T. Pavia. 2015. Community Surveillance of Respiratory Viruses Among Families in the Utah Better Identification of Germs-Longitudinal Viral Epidemiology (BIG-LoVE) Study. *Clin. Infect. Dis.* 61:1217–1224. http://dx.doi.org/10.1093/cid/civ486

Casanova, J.L., M.E. Conley, S.J. Seligman, L. Abel, and L.D. Notarangelo. 2014. Guidelines for genetic studies in single patients: lessons from primary immunodeficiencies. *J. Exp. Med.* 211:2137–2149. http://dx.doi.org/10.1084/jem.20140520

Case, D.A., J.T. Berryman, R.M. Betz, D.S. Cerutti, and I. Cheatham. T.E., T.A. Darden, R.E. Duke, T.J. Giese, H. Gohlke, A.W. Goetz, N. Homeyer, S. Izadi, P. Janowski, J. Kaus, A. Kovalenko, T.S. Lee, S. LeGrand, P. Li, T. Luchko, R. Luo, B. Madej, K.M. Merz, G. Monard, P. Needham, H. Nguyen, H.T. Nguyen, I. Omelyan, A. Onufriev, D.R. Roe, A. Roitberg, R. Salomon-Ferrer, C.L. Simmerling, W. Smith, J. Swails, R.C. Walker, J. Wang, R.M. Wolf, X. Wu, D.M. York, and P.A. Kollman. 2015. AMBER 2015. In University of California, San Francisco.

Chapgier, A., R.F. Wynn, E. Jouanguy, O. Filipe-Santos, S. Zhang, J. Feinberg, K. Hawkins, J.L. Casanova, and P.D. Arkwright. 2006. Human complete Stat-1 deficiency is associated with defective type I and II IFN responses in vitro but immunity to some low virulence viruses in vivo. *J. Immunol.* 176:5078–5083. http://dx.doi.org/10.4049/jimmunol.176.8.5078

Ciancanelli, M.J., S.X. Huang, P. Luthra, H. Garner, Y. Itan, S. Volpi, F.G. Lafaille, C. Trouillet, M. Schmolke, R.A. Albrecht, et al. 2015. Infectious disease. Life-threatening influenza and impaired interferon amplification in human IRF7 deficiency. *Science.* 348:448–453. http://dx.doi.org/10.1126/science.aaa1578

de Chasseval, R., and J.P. de Villartay. 1992. High level transient gene expression in human lymphoid cells by SV40 large T antigen boost. *Nucleic Acids Res.* 20:245–250. http://dx.doi.org/10.1093/nar/20.2.245

Delaloye, J., T. Roger, Q.G. Steiner-Tardivel, D. Le Roy, M. Knaup Reymond, S. Akira, V. Petrilli, C.E. Gomez, B. Perdiguero, J. Tschopp, et al. 2009. Innate immune sensing of modified vaccinia virus Ankara (MVA) is mediated by TLR2-TLR6, MDA-5 and the NALP3 inflammasome. *PLoS Pathog.* 5:e1000480. http://dx.doi.org/10.1371/journal.ppat.1000480

Deschamps, M., G. Laval, M. Fagny, Y. Itan, L. Abel, J.L. Casanova, E. Patin, and L. Quintana-Murci. 2016. Genomic Signatures of Selective Pressures and Introgression from Archaic Hominins at Human Innate Immunity Genes. *Am. J. Hum. Genet.* 98:5–21. http://dx.doi.org/10.1016/j.ajhg.2015.11.014

Dittmann, M., H.H. Hoffmann, M.A. Scull, R.H. Gilmore, K.L. Bell, M. Ciancanelli, S.J. Wilson, S. Crotta, Y. Yu, B. Flatley, et al. 2015. A serpin shapes the extracellular environment to prevent influenza A virus maturation. *Cell.* 160:631–643. http://dx.doi.org/10.1016/j.cell.2015.01.040

Eilertson, K.E., J.G. Booth, and C.D. Bustamante. 2012. SnIPRE: selection inference using a Poisson random effects model. *PLOS Comput. Biol.* 8:e1002806. http://dx.doi.org/10.1371/journal.pcbi.1002806

Errett, J.S., M.S. Suthar, A. McMillan, M.S. Diamond, and M. Gale Jr. 2013. The essential, nonredundant roles of RIG-I and MDA5 in detecting and controlling West Nile virus infection. *J. Virol.* 87:11416–11425. http://dx.doi.org/10.1128/JVI.01488-13

Galama, J.M., M. Gielen, and C.M. Weemaes. 2000. Enterovirus antibody titers after IVIG replacement in agammaglobulinemic children. *Clin. Microbiol. Infect.* 6:630–632. http://dx.doi.org/10.1046/j.1469-0691.2000.00173.x

Gaunt, E.R., H. Harvala, C. McIntyre, K.E. Templeton, and P. Simmonds. 2011. Disease burden of the most commonly detected respiratory viruses in hospitalized patients calculated using the disability adjusted life year (DALY) model. *J. Clin. Virol.* 52:215–221. http://dx.doi.org/10.1016/j.jcv.2011.07.017

Gitlin, L., W. Barchet, S. Gilfillan, M. Cella, B. Beutler, R.A. Flavell, M.S. Diamond, and M. Colonna. 2006. Essential role of mda-5 in type I IFN responses to polyriboinosinic:polyribocytidylic acid and encephalomyocarditis picornavirus. *Proc. Natl. Acad. Sci. USA.* 103:8459–8464. http://dx.doi.org/10.1073/pnas.0603082103

Gitlin, L., L. Benoit, C. Song, M. Cella, S. Gilfillan, M.J. Holtzman, and M. Colonna. 2010. Melanoma differentiation-associated gene 5 (MDA5) is involved in the innate immune response to Paramyxoviridae infection in vivo. *PLoS Pathog.* 6:e1000734. http://dx.doi.org/10.1371/journal.ppat.1000734

Global Burden of Disease Study 2013 Collaborators. 2015. Global, regional, and national incidence, prevalence, and years lived with disability for 301 acute and chronic diseases and injuries in 188 countries, 1990-2013: a systematic analysis for the Global Burden of Disease Study 2013. *Lancet.* 386:743–800. http://dx.doi.org/10.1016/S0140-6736(15)60692-4

Grandvaux, N., X. Guan, F. Yoboua, N. Zucchini, K. Fink, P. Doyon, L. Martin, M.J. Servant, and S. Chartier. 2014. Sustained activation of interferon regulatory factor 3 during infection by paramyxoviruses requires MDA5. *J. Innate Immun.* 6:650–662. http://dx.doi.org/10.1159/000360764

Greenberg, S.B. 2011. Update on rhinovirus and coronavirus infections. *Semin. Respir. Crit. Care Med.* 32:433–446. http://dx.doi.org/10.1055/s-0031-1283283

Hanawa, H., P. Hematti, K. Keyvanfar, M.E. Metzger, A. Krouse, R.E. Donahue, S. Kepes, J. Gray, C.E. Dunbar, D.A. Persons, and A.W. Nienhuis. 2004. Efficient gene transfer into rhesus repopulating hematopoietic stem cells using a simian immunodeficiency virus-based lentiviral vector system. *Blood.* 103:4062–4069. http://dx.doi.org/10.1182/blood-2004-01-0045

Hasegawa, K., J.M. Mansbach, and C.A. Camargo Jr. 2014. Infectious pathogens and bronchiolitis outcomes. *Expert Rev. Anti Infect. Ther.* 12:817–828. http://dx.doi.org/10.1586/14787210.2014.906901

Heikkinen, T., and A. Järvinen. 2003. The common cold. *Lancet.* 361:51–59. http://dx.doi.org/10.1016/S0140-6736(03)12162-9

Hornak, V., R. Abel, A. Okur, B. Strockbine, A. Roitberg, and C. Simmerling. 2006. Comparison of multiple Amber force fields and development of improved protein backbone parameters. *Proteins.* 65:712–725. http://dx.doi.org/10.1002/prot.21123

Israel, L., Y. Wang, K. Bulek, E. Della Mina, Z. Zhang, V. Pedergnana, M. Chrabieh, N.A. Lemmens, V. Sancho-Shimizu, M. Descatoire, et al. 2017. Human Adaptive Immunity Rescues an Inborn Error of Innate Immunity. *Cell.* 168:789–800.e10. http://dx.doi.org/10.1016/j.cell.2017.01.039

Itan, Y., L. Shang, B. Boisson, M.J. Ciancanelli, J.G. Markle, R. Martinez-Barricarte, E. Scott, I. Shah, P.D. Stenson, J. Gleeson, et al. 2016. The mutation significance cutoff: gene-level thresholds for variant predictions. *Nat. Methods.* 13:109–110. http://dx.doi.org/10.1038/nmeth.3739

Jaïdane, H., P. Sauter, F. Sane, A. Goffard, J. Gharbi, and D. Hober. 2010. Enteroviruses and type 1 diabetes: towards a better understanding of the relationship. *Rev. Med. Virol.* 20:265–280. http://dx.doi.org/10.1002/rmv.647

Jain, S., D.J. Williams, S.R. Arnold, K. Ampofo, A.M. Bramley, C. Reed, C. Stockmann, E.J. Anderson, C.G. Grijalva, W.H. Self, et al. CDC EPIC Study Team. 2015. Community-acquired pneumonia requiring hospitalization among U.S. children. *N. Engl. J. Med.* 372:835–845. http://dx.doi.org/10.1056/NEJMoa1405870

Jin, Y.H., S.J. Kim, E.Y. So, L. Meng, M. Colonna, and B.S. Kim. 2012. Melanoma differentiation-associated gene 5 is critical for protection against Theiler's virus-induced demyelinating disease. *J. Virol.* 86:1531–1543. http://dx.doi.org/10.1128/JVI.06457-11

Jing, H., Q. Zhang, Y. Zhang, B.J. Hill, C.G. Dove, E.W. Gelfand, T.P. Atkinson, G. Uzel, H.F. Matthews, P.J. Mustillo, et al. 2014. Somatic reversion in dedicator of cytokinesis 8 immunodeficiency modulates disease phenotype. *J. Allergy Clin. Immunol.* 133:1667–1675. http://dx.doi.org/10.1016/j.jaci.2014.03.025

Kato, H., O. Takeuchi, S. Sato, M. Yoneyama, M. Yamamoto, K. Matsui, S. Uematsu, A. Jung, T. Kawai, K.J. Ishii, et al. 2006. Differential roles of MDA5 and RIG-I helicases in the recognition of RNA viruses. *Nature.* 441:101–105. http://dx.doi.org/10.1038/nature04734

Kim, W.K., D. Jain, M.D. Sánchez, C.J. Koziol-White, K. Matthews, M.Q. Ge, A. Haczku, R.A. Panettieri Jr., M.B. Frieman, and C.B. López. 2014. Deficiency of melanoma differentiation-associated protein 5 results in exacerbated chronic postviral lung inflammation. *Am. J. Respir. Crit. Care Med.* 189:437–448. http://dx.doi.org/10.1164/rccm.201307-1338OC

Kingston, R.E., C.A. Chen, and H. Okayama. 2003. Calcium phosphate transfection. *Curr Protoc Cell Biol* Chapter 20:Unit 20 23.

Lee, W.M., Y. Chen, W. Wang, and A. Mosser. 2015a. Growth of human rhinovirus in H1-HeLa cell suspension culture and purification of virions. *Methods Mol. Biol.* 1221:49–61. http://dx.doi.org/10.1007/978-1-4939-1571-2_5

Lee, W.M., Y. Chen, W. Wang, and A. Mosser. 2015b. Infectivity assays of human rhinovirus-A and -B serotypes. *Methods Mol. Biol.* 1221:71–81. http://dx.doi.org/10.1007/978-1-4939-1571-2_7

Lee, W.M., K. Grindle, R. Vrtis, T. Pappas, F. Vang, I. Lee, and J.E. Gern. 2015c. Molecular identification and quantification of human rhinoviruses in respiratory samples. *Methods Mol. Biol.* 1221:25–38. http://dx.doi.org/10.1007/978-1-4939-1571-2_3

Li, J., Y. Liu, and X. Zhang. 2010. Murine coronavirus induces type I interferon in oligodendrocytes through recognition by RIG-I and MDA5. *J. Virol.* 84:6472–6482. http://dx.doi.org/10.1128/JVI.00016-10

Li, P., B.P. Roberts, D.K. Chakravorty, and K.M. Merz Jr. 2013. Rational Design of Particle Mesh Ewald Compatible Lennard-Jones Parameters for +2 Metal Cations in Explicit Solvent. *J. Chem. Theory Comput.* 9:2733–2748. http://dx.doi.org/10.1021/ct400146w

Lin, R., P. Génin, Y. Mamane, and J. Hiscott. 2000. Selective DNA binding and association with the CREB binding protein coactivator contribute to differential activation of alpha/beta interferon genes by interferon regulatory factors 3 and 7. *Mol. Cell. Biol.* 20:6342–6353. http://dx.doi.org/10.1128/MCB.20.17.6342-6353.2000

Loo, Y.M., J. Fornek, N. Crochet, G. Bajwa, O. Perwitasari, L. Martinez-Sobrido, S. Akira, M.A. Gill, A. García-Sastre, M.G. Katze, and M. Gale Jr. 2008. Distinct RIG-I and MDA5 signaling by RNA viruses in innate immunity. *J. Virol.* 82:335–345. http://dx.doi.org/10.1128/JVI.01080-07

Mäkelä, M.J., T. Puhakka, O. Ruuskanen, M. Leinonen, P. Saikku, M. Kimpimäki, S. Blomqvist, T. Hyypiä, and P. Arstila. 1998. Viruses and bacteria in the etiology of the common cold. *J. Clin. Microbiol.* 36:539–542.

McCartney, S.A., L.B. Thackray, L. Gitlin, S. Gilfillan, H.W. Virgin, and M. Colonna. 2008. MDA-5 recognition of a murine norovirus. *PLoS Pathog.* 4:e1000108. http://dx.doi.org/10.1371/journal.ppat.1000108

McCartney, S.A., W. Vermi, S. Lonardi, C. Rossini, K. Otero, B. Calderon, S. Gilfillan, M.S. Diamond, E.R. Unanue, and M. Colonna. 2011. RNA sensor-induced type I IFN prevents diabetes caused by a β cell-tropic virus in mice. *J. Clin. Invest.* 121:1497–1507. http://dx.doi.org/10.1172/JCI44005

McQuillan, R., A.L. Leutenegger, R. Abdel-Rahman, C.S. Franklin, M. Pericic, L. Barac-Lauc, N. Smolej-Narancic, B. Janicijevic, O. Polasek, A. Tenesa, et al. 2008. Runs of homozygosity in European populations. *Am. J. Hum. Genet.* 83:359–372. http://dx.doi.org/10.1016/j.ajhg.2008.08.007

Meagher, K.L., L.T. Redman, and H.A. Carlson. 2003. Development of polyphosphate parameters for use with the AMBER force field. *J. Comput. Chem.* 24:1016–1025. http://dx.doi.org/10.1002/jcc.10262

Munir, S., C. Le Nouen, C. Luongo, U.J. Buchholz, P.L. Collins, and A. Bukreyev. 2008. Nonstructural proteins 1 and 2 of respiratory syncytial virus suppress maturation of human dendritic cells. *J. Virol.* 82:8780–8796. http://dx.doi.org/10.1128/JVI.00630-08

Nejentsev, S., N. Walker, D. Riches, M. Egholm, and J.A. Todd. 2009. Rare variants of IFIH1, a gene implicated in antiviral responses, protect against type 1 diabetes. *Science.* 324:387–389. http://dx.doi.org/10.1126/science.1167728

Oda, H., K. Nakagawa, J. Abe, T. Awaya, M. Funabiki, A. Hijikata, R. Nishikomori, M. Funatsuka, Y. Ohshima, Y. Sugawara, et al. 2014. Aicardi-Goutières syndrome is caused by IFIH1 mutations. *Am. J. Hum. Genet.* 95:121–125. http://dx.doi.org/10.1016/j.ajhg.2014.06.007

Palmenberg, A.C., D. Spiro, R. Kuzmickas, S. Wang, A. Djikeng, J.A. Rathe, C.M. Fraser-Liggett, and S.B. Liggett. 2009. Sequencing and analyses of all known human rhinovirus genomes reveal structure and evolution. *Science.* 324:55–59. http://dx.doi.org/10.1126/science.1165557

Pavia, A.T. 2011. Viral infections of the lower respiratory tract: old viruses, new viruses, and the role of diagnosis. *Clin. Infect. Dis.* 52(Suppl 4):S284–S289. http://dx.doi.org/10.1093/cid/cir043

Pichlmair, A., O. Schulz, C.P. Tan, J. Rehwinkel, H. Kato, O. Takeuchi, S. Akira, M. Way, G. Schiavo, and C. Reis e Sousa. 2009. Activation of MDA5 requires higher-order RNA structures generated during virus infection. *J. Virol.* 83:10761–10769. http://dx.doi.org/10.1128/JVI.00770-09

Poole, A., C. Urbanek, C. Eng, J. Schageman, S. Jacobson, B.P. O'Connor, J.M. Galanter, C.R. Gignoux, L.A. Roth, R. Kumar, et al. 2014. Dissecting childhood asthma with nasal transcriptomics distinguishes subphenotypes of disease. *J. Allergy Clin. Immunol.* 133:670–8.e12. http://dx.doi.org/10.1016/j.jaci.2013.11.025

Purcell, S., B. Neale, K. Todd-Brown, L. Thomas, M.A. Ferreira, D. Bender, J. Maller, P. Sklar, P.I. de Bakker, M.J. Daly, and P.C. Sham. 2007. PLINK: a tool set for whole-genome association and population-based linkage analyses. *Am. J. Hum. Genet.* 81:559–575. http://dx.doi.org/10.1086/519795

Retterer, K., J. Juusola, M.T. Cho, P. Vitazka, F. Millan, F. Gibellini, A. Vertino-Bell, N. Smaoui, J. Neidich, K.G. Monaghan, et al. 2016. Clinical application of whole-exome sequencing across clinical indications. *Genet. Med.* 18:696–704. http://dx.doi.org/10.1038/gim.2015.148

Reynolds, S.D., C. Rios, A. Wesolowska-Andersen, Y. Zhuang, M. Pinter, C. Happoldt, C.L. Hill, S.W. Lallier, G.P. Cosgrove, G.M. Solomon, et al. 2016. Airway Progenitor Clone Formation Is Enhanced by Y-27632-Dependent Changes in the Transcriptome. *Am. J. Respir. Cell Mol. Biol.* 55:323–336. http://dx.doi.org/10.1165/rcmb.2015-0274MA

Rice, G.I., G.M. Forte, M. Szynkiewicz, D.S. Chase, A. Aeby, M.S. Abdel-Hamid, S. Ackroyd, R. Allcock, K.M. Bailey, U. Balottin, et al. 2013. Assessment of interferon-related biomarkers in Aicardi-Goutières syndrome associated with mutations in TREX1, RNASEH2A, RNASEH2B, RNASEH2C, SAMHD1, and ADAR: a case-control study. *Lancet Neurol.* 12:1159–1169. http://dx.doi.org/10.1016/S1474-4422(13)70258-8

Rice, G.I., Y. del Toro Duany, E.M. Jenkinson, G.M. Forte, B.H. Anderson, G. Ariaudo, B. Bader-Meunier, E.M. Baildam, R. Battini, M.W. Beresford, et al. 2014. Gain-of-function mutations in IFIH1 cause a spectrum of human disease phenotypes associated with upregulated type I interferon signaling. *Nat. Genet.* 46:503–509. http://dx.doi.org/10.1038/ng.2933

Rodero, M.P., and Y.J. Crow. 2016. Type I interferon-mediated monogenic autoinflammation: The type I interferonopathies, a conceptual overview. *J. Exp. Med.* 213:2527–2538. http://dx.doi.org/10.1084/jem.20161596

Rodriguez-Calvo, T., and M.G. von Herrath. 2015. Enterovirus infection and type 1 diabetes: closing in on a link? *Diabetes.* 64:1503–1505. http://dx.doi.org/10.2337/db14-1931

Roth-Cross, J.K., S.J. Bender, and S.R. Weiss. 2008. Murine coronavirus mouse hepatitis virus is recognized by MDA5 and induces type I

interferon in brain macrophages/microglia. *J. Virol.* 82:9829–9838. http://dx.doi.org/10.1128/JVI.01199-08

Rutsch, F., M. MacDougall, C. Lu, I. Buers, O. Mamaeva, Y. Nitschke, G.I. Rice, H. Erlandsen, H.G. Kehl, H. Thiele, et al. 2015. A specific IFIH1 gain-of-function mutation causes Singleton-Merten syndrome. *Am. J. Hum. Genet.* 96:275–282. http://dx.doi.org/10.1016/j.ajhg.2014.12.014

Salomon-Ferrer, R., A.W. Goetz, D. Poole, S. Le Grand, and R.C. Walker. 2013. Routine microsecond molecular dynamics simulations with AMBER – Part II: Particle Mesh Ewald. *J. Chem. Theory Comput.* 9:3878–3888. http://dx.doi.org/10.1021/ct400314y

Shingai, M., T. Ebihara, N.A. Begum, A. Kato, T. Honma, K. Matsumoto, H. Saito, H. Ogura, M. Matsumoto, and T. Seya. 2007. Differential type I IFN-inducing abilities of wild-type versus vaccine strains of measles virus. *J. Immunol.* 179:6123–6133. http://dx.doi.org/10.4049/jimmunol.179.9.6123

Sirén, J., T. Imaizumi, D. Sarkar, T. Pietilä, D.L. Noah, R. Lin, J. Hiscott, R.M. Krug, P.B. Fisher, I. Julkunen, and S. Matikainen. 2006. Retinoic acid inducible gene-I and mda-5 are involved in influenza A virus-induced expression of antiviral cytokines. *Microbes Infect.* 8:2013–2020. http://dx.doi.org/10.1016/j.micinf.2006.02.028

Slater, L., N.W. Bartlett, J.J. Haas, J. Zhu, S.D. Message, R.P. Walton, A. Sykes, S. Dahdaleh, D.L. Clarke, M.G. Belvisi, et al. 2010. Co-ordinated role of TLR3, RIG-I and MDA5 in the innate response to rhinovirus in bronchial epithelium. *PLoS Pathog.* 6:e1001178. http://dx.doi.org/10.1371/journal.ppat.1001178

Smyth, D.J., J.D. Cooper, R. Bailey, S. Field, O. Burren, L.J. Smink, C. Guja, C. Ionescu-Tirgoviste, B. Widmer, D.B. Dunger, et al. 2006. A genome-wide association study of nonsynonymous SNPs identifies a type 1 diabetes locus in the interferon-induced helicase (IFIH1) region. *Nat. Genet.* 38:617–619. http://dx.doi.org/10.1038/ng1800

Stewart, S.A., D.M. Dykxhoorn, D. Palliser, H. Mizuno, E.Y. Yu, D.S. An, D.M. Sabatini, I.S. Chen, W.C. Hahn, P.A. Sharp, et al. 2003. Lentivirus-delivered stable gene silencing by RNAi in primary cells. *RNA.* 9:493–501. http://dx.doi.org/10.1261/rna.2192803

Sulem, P., H. Helgason, A. Oddson, H. Stefansson, S.A. Gudjonsson, F. Zink, E. Hjartarson, G.T. Sigurdsson, A. Jonasdottir, A. Jonasdottir, et al. 2015. Identification of a large set of rare complete human knockouts. *Nat. Genet.* 47:448–452. http://dx.doi.org/10.1038/ng.3243

Suprynowicz, F.A., G. Upadhyay, E. Krawczyk, S.C. Kramer, J.D. Hebert, X. Liu, H. Yuan, C. Cheluvaraju, P.W. Clapp, R.C. Boucher Jr., et al. 2012. Conditionally reprogrammed cells represent a stem-like state of adult epithelial cells. *Proc. Natl. Acad. Sci. USA.* 109:20035–20040. http://dx.doi.org/10.1073/pnas.1213241109

Triantafilou, K., E. Vakakis, E.A. Richer, G.L. Evans, J.P. Villiers, and M. Triantafilou. 2011. Human rhinovirus recognition in non-immune cells is mediated by Toll-like receptors and MDA-5, which trigger a synergetic pro-inflammatory immune response. *Virulence.* 2:22–29. http://dx.doi.org/10.4161/viru.2.1.13807

Van Eyck, L., L. De Somer, D. Pombal, S. Bornschein, G. Frans, S. Humblet-Baron, L. Moens, F. de Zegher, X. Bossuyt, C. Wouters, and A. Liston. 2015. IFIH1 mutation causes systemic lupus erythematosus with selective IgA-deficiency. *Arthritis Rheumatol.* 67:1592–1597. http://dx.doi.org/10.1002/art.39110

Wang, J.P., A. Cerny, D.R. Asher, E.A. Kurt-Jones, R.T. Bronson, and R.W. Finberg. 2010. MDA5 and MAVS mediate type I interferon responses to coxsackie B virus. *J. Virol.* 84:254–260. http://dx.doi.org/10.1128/JVI.00631-09

Wang, Q., D.R. Nagarkar, E.R. Bowman, D. Schneider, B. Gosangi, J. Lei, Y. Zhao, C.L. McHenry, R.V. Burgens, D.J. Miller, et al. 2009. Role of double-stranded RNA pattern recognition receptors in rhinovirus-induced airway epithelial cell responses. *J. Immunol.* 183:6989–6997. http://dx.doi.org/10.4049/jimmunol.0901386

Wang, Q., D.J. Miller, E.R. Bowman, D.R. Nagarkar, D. Schneider, Y. Zhao, M.J. Linn, A.M. Goldsmith, J.K. Bentley, U.S. Sajjan, and M.B. Hershenson. 2011. MDA5 and TLR3 initiate pro-inflammatory signaling pathways leading to rhinovirus-induced airways inflammation and hyperresponsiveness. *PLoS Pathog.* 7:e1002070. http://dx.doi.org/10.1371/journal.ppat.1002070

Wiszniewski, W., J.V. Hunter, N.A. Hanchard, J.R. Willer, C. Shaw, Q. Tian, A. Illner, X. Wang, S.W. Cheung, A. Patel, et al. 2013. TM4SF20 ancestral deletion and susceptibility to a pediatric disorder of early language delay and cerebral white matter hyperintensities. *Am. J. Hum. Genet.* 93:197–210. http://dx.doi.org/10.1016/j.ajhg.2013.05.027

Wu, B., A. Peisley, C. Richards, H. Yao, X. Zeng, C. Lin, F. Chu, T. Walz, and S. Hur. 2013. Structural basis for dsRNA recognition, filament formation, and antiviral signal activation by MDA5. *Cell.* 152:276–289. http://dx.doi.org/10.1016/j.cell.2012.11.048

Yang, Y., D.M. Muzny, J.G. Reid, M.N. Bainbridge, A. Willis, P.A. Ward, A. Braxton, J. Beuten, F. Xia, Z. Niu, et al. 2013. Clinical whole-exome sequencing for the diagnosis of mendelian disorders. *N. Engl. J. Med.* 369:1502–1511. http://dx.doi.org/10.1056/NEJMoa1306555

Yang, Y., D.M. Muzny, F. Xia, Z. Niu, R. Person, Y. Ding, P. Ward, A. Braxton, M. Wang, C. Buhay, et al. 2014. Molecular findings among patients referred for clinical whole-exome sequencing. *JAMA.* 312:1870–1879. http://dx.doi.org/10.1001/jama.2014.14601

Züst, R., L. Cervantes-Barragan, M. Habjan, R. Maier, B.W. Neuman, J. Ziebuhr, K.J. Szretter, S.C. Baker, W. Barchet, M.S. Diamond, et al. 2011. Ribose 2′-O-methylation provides a molecular signature for the distinction of self and non-self mRNA dependent on the RNA sensor Mda5. *Nat. Immunol.* 12:137–143. http://dx.doi.org/10.1038/ni.1979